

# Institutionen för systemteknik

## Department of Electrical Engineering

**Examensarbete**

### **Extended Kalman Filter for Robust UAV Attitude Estimation**

Examensarbete utfört i Reglerteknik  
vid Tekniska högskolan vid Linköpings universitet  
av

**Martin Pettersson**

LiTH-ISY-EX-15/4835-SE

Linköping 2015



**Linköpings universitet**  
**TEKNISKA HÖGSKOLAN**



# **Extended Kalman Filter for Robust UAV Attitude Estimation**

Examensarbete utfört i Reglerteknik  
vid Tekniska högskolan vid Linköpings universitet  
av

**Martin Pettersson**

LiTH-ISY-EX-15/4835-SE

Handledare:   **Clas Veibäck**  
                          ISY, Linköpings universitet  
**Thom Magnusson**  
                          UAS Europe

Examinator:   **Fredrik Gustafsson**  
                          ISY, Linköpings universitet

Linköping, 9 juni 2015





**Avdelning, Institution**  
Division, Department

Division of Automatic Control  
Department of Electrical Engineering  
SE-581 83 Linköping

**Datum**  
Date

2015-06-09

**Språk**

Language

Svenska/Swedish

Engelska/English

\_\_\_\_\_

**Rapporttyp**

Report category

Licentiatavhandling

Examensarbete

C-uppsats

D-uppsats

Övrig rapport

\_\_\_\_\_

**ISBN**

\_\_\_\_\_

**ISRN**

LiTH-ISY-EX-15/4835-SE

**Serietitel och serienummer**  
Title of series, numbering

**ISSN**

\_\_\_\_\_

**URL för elektronisk version**

<http://www.ep.liu.se>

**Titel**

Title

Extended Kalmanfilter för robust estimering av UAV-attityd

Extended Kalman Filter for Robust UAV Attitude Estimation

**Författare**

Martin Pettersson

Author

**Sammanfattning**

Abstract

Attitude estimation of unmanned aerial vehicles is of great importance as it enables proper control of the vehicles. Attitude estimation is typically done by an *attitude-heading reference system* (AHRS) which utilises different kind of sensors. In this thesis these include a gyroscope providing angular rates measurements which can be integrated to describe the attitude as well as an accelerometer and a magnetometer, both of which can be compared with known reference vectors to determine the attitude. The sensor measurements are fused using a GPS augmented 7-state *Extended Kalman filter* (EKF) with a quaternion and gyroscope biases as state variables. It uses differentiated GPS velocity measurements to estimate external accelerations as reference vector to the accelerometer, which significantly raises robustness of the solution. The filter is implemented in Matlab™ and in c on an ARM microprocessor. It is compared with an explicit complementary filter solution and is evaluated with flights using a fixed-wing UAV with satisfactory results.

**Nyckelord**

Keywords

Kalman, autonomous, UAV, EKF, attitude, INS, IMU



## **Sammanfattning**

Estimering av attityden hos obemannade farkoster är av stor vikt för att bra reglering ska kunna göras. Estimering av attityden görs av ett system kallat AHRS vilket använder sig av olika sensorer. Dessa sensorer inkluderar gyroskop som integreras för att beskriva attityden samt accelerometer och magnetometer vilka används för att jämföras med kända referensvektorer och på så vis rikta in attityden och kompensera för fel från gyroskopets bias. I detta examensarbetet estimeras attityden med ett GPS-kompenserat 7-tillståndigt *Extended Kalman filter* (EKF) med en kvaternion och gyroskopbias som tillstånd. Det använder differentierad GPS-hastighet för kompensering av externa accelerationer, vilket medför en signifikant förbättring i robusthet. Det är implementerat i Matlab™ och i c på en ARM-microprosessor. Filtret utvärderas genom jämförelse med ett komplett filter på både test-bänk och flygning med ett RC-flygplan och påvisar goda egenskaper.



## Abstract

Attitude estimation of unmanned aerial vehicles is of great importance as it enables proper control of the vehicles. Attitude estimation is typically done by an *attitude-heading reference system* (AHRS) which utilises different kind of sensors. In this thesis these include a gyroscope providing angular rates measurements which can be integrated to describe the attitude as well as an accelerometer and a magnetometer, both of which can be compared with known reference vectors to determine the attitude. The sensor measurements are fused using a GPS augmented 7-state *Extended Kalman filter* (EKF) with a quaternion and gyroscope biases as state variables. It uses differentiated GPS velocity measurements to estimate external accelerations as reference vector to the accelerometer, which significantly raises robustness of the solution. The filter is implemented in Matlab<sup>TM</sup> and in c on an ARM microprocessor. It is compared with an explicit complementary filter solution and is evaluated with flights using a fixed-wing UAV with satisfactory results.



## Acknowledgments

There are a lot of people who have made this thesis possible that i would like to thank. First I'd like to thank the people at UAS Europe and my supervisor Thom Magnusson whom have helped me a great deal during the thesis. I would also like to thank my supervisor at ISY, Clas Veibäck who have provided good ideas and input on how to improve my work. And thanks to my examiner Fredrik Gustafsson who found time to help during the thesis, which is admirable and for which I'm grateful. Lastly I would like to thank my girlfriend Elin for keeping my spirits up.

*Linköping, May 2015  
Martin Pettersson*



---

# Contents

<b>Notation</b>	<b>xiii</b>
<b>1 Introduction</b>	<b>1</b>
1.1 Background . . . . .	1
1.1.1 Similar Work . . . . .	2
1.2 Market and Methods . . . . .	3
1.3 Motivation . . . . .	4
1.4 Previous Solution . . . . .	5
<b>2 Coordinate Systems</b>	<b>7</b>
2.1 Geodetic Frame, WGS . . . . .	8
2.2 Earth-Centred-Earth-Fixed Frame, ECEF . . . . .	9
2.3 North-East-Down Frame, NED . . . . .	9
2.4 Body Frame, $B$ . . . . .	9
2.5 Rotational Concepts . . . . .	10
2.5.1 Euler Angles, Tait-Bryant Angles . . . . .	10
2.5.2 Quaternion Representation . . . . .	12
2.5.3 Relationship Between Quaternions and Euler Angles . . . . .	15
<b>3 Sensors</b>	<b>17</b>
3.1 Hardware . . . . .	17
3.2 Sensor Performance . . . . .	18
3.2.1 Random Walk . . . . .	18
3.2.2 Inter-Sensor Misalignment . . . . .	18
3.3 Gyroscope . . . . .	19
3.3.1 Performance . . . . .	19
3.3.2 Analysis . . . . .	20
3.3.3 Calibration . . . . .	22
3.4 Accelerometer . . . . .	23
3.4.1 Performance . . . . .	23
3.4.2 Analysis . . . . .	23
3.4.3 Calibration . . . . .	25
3.5 Magnetometer . . . . .	30

3.5.1	Performance . . . . .	31
3.5.2	Calibration . . . . .	32
3.6	GPS Module . . . . .	35
3.6.1	Performance . . . . .	36
3.6.2	Analysis . . . . .	36
3.7	Sensor-Platform Performance . . . . .	39
3.7.1	Vibrations . . . . .	39
3.7.2	Magnetic Disturbances . . . . .	40
<b>4</b>	<b>Sensor Models</b>	<b>41</b>
4.1	System Dynamics . . . . .	41
4.2	Accelerometer . . . . .	42
4.3	Magnetometer . . . . .	43
4.4	Linearization and Discretization . . . . .	43
4.4.1	System Dynamics . . . . .	43
4.4.2	Measurement Model . . . . .	43
4.5	Problems . . . . .	45
4.5.1	Magnetometer Sensitivity . . . . .	45
4.5.2	Accelerated Motion . . . . .	46
4.6	Magnetic Modelling . . . . .	47
<b>5</b>	<b>Extended Kalman Filter</b>	<b>49</b>
5.1	Theory . . . . .	49
5.2	The Extended Kalman Filter . . . . .	50
5.3	Iterated Kalman . . . . .	51
5.4	Observability . . . . .	51
5.4.1	Monitoring EKF Performance . . . . .	52
<b>6</b>	<b>Implementation</b>	<b>55</b>
6.1	EasyPilot 3.0 . . . . .	55
6.2	Computational Complexity . . . . .	55
6.3	Initialisation . . . . .	56
6.4	Pre-processing . . . . .	56
<b>7</b>	<b>Results</b>	<b>57</b>
7.1	Tests . . . . .	57
7.2	Test bench . . . . .	58
7.2.1	Static tests . . . . .	58
7.2.2	Magnetic Disturbance Tests . . . . .	58
7.2.3	Acceleration Tests . . . . .	60
7.2.4	Dynamic Tests . . . . .	62
7.2.5	Sensor Calibration and Misalignment . . . . .	63
7.3	Flight Tests . . . . .	65
7.3.1	Acceleration Tests . . . . .	66
7.3.2	Filter Convergence . . . . .	69
7.4	Implemented Filter . . . . .	69
7.4.1	Test Bench . . . . .	69

7.4.2	Flight Tests . . . . .	70
7.5	Magnetic Modelling . . . . .	74
7.6	Evaluation . . . . .	75
<b>8</b>	<b>Conclusion</b>	<b>77</b>
8.1	Conclusions . . . . .	77
8.2	Future Work . . . . .	77
8.2.1	UKF . . . . .	78
8.2.2	Accelerometer Bias . . . . .	78
8.2.3	Misalignment . . . . .	78
8.2.4	Filter Monitor . . . . .	78
8.2.5	Magnetic Modelling . . . . .	78
<b>A</b>	<b>Appendix A</b>	<b>81</b>
A.1	Transformations . . . . .	81
A.1.1	Geodetic and ECEF . . . . .	81
A.1.2	ECEF to NED . . . . .	81
	<b>Bibliography</b>	<b>83</b>



---

# Notation

## ABBREVIATIONS

Abbreviation	Meaning
AHRS	Attitude-Heading Reference System
AMR	Anisotropic Magnetoresistive (magnetometer)
B	Body (frame)
DCM	Direction Cosine Matrix
ECEF	Earth-Centered Earth-Fixed (frame)
ECF	Explicit Complementary Filter
EKF	Extended Kalman Filter
GCS	World Geodetic System
GNSS	Global Navigation Satellite System
GPS	Global Positioning System
IMU	Inertial Measurement Unit
KF	Kalman Filter
LP	Low-Pass
LS	Least Squares
MEMS	Micro-Electro Mechanical Systems (technology)
NED	North-East-Down (frame)
UAV	Unmanned Aerial Vehicle
UKF	Unscented Kalman filter
WGS	World Geodetic System

---



# 1

---

## Introduction

### 1.1 Background

The field of unmanned flight is growing every day. UAVs are used in various applications, from security and military to sport events and leisure activities. The market is growing and new ways to use the technology are discovered at a fast pace. All fields concerning UAVs enforce a need of security. The vehicles must be able to operate in dangerous areas which might lead to malfunctioning sensor equipment and they must have a reliable way of determining how they are positioned and oriented in the world. Without this reliability the use of UAVs would be slim.

Navigation and attitude estimation is well researched and is covered thoroughly in literature which allows several methods to be chosen from. The purpose of the thesis is to estimate the attitude of a small-scale aircraft by using inertial sensors with the aid of other sensors. To estimate the attitude in a controlled environment is a task that can be solved in numerous ways. The task of estimating the attitude with disturbances and during acrobatic manoeuvres is however another matter.

Typical flight models are highly non-linear which is why a traditional *Kalman filter* (KF) can not be used. These non-linearities have to be handled by a framework which allows non-linear equations. According to Crassidis et al. [2007] the oldest and most common approach which was first used in the Apollo project is the *Extended Kalman filter* (EKF) which handles the non-linearities by linearization at the current state estimate, but there are a multitude of other filters which can be applied. Another common approach is the *Unscented Kalman filter* (UKF) which have successfully been applied in de Marina et al. [2012]. However, Crassidis et al. [2007] concludes that the EKF is preferred in most situations due to the flexibility of the approach. The UKF handles severe non-linearities better and

does not need a good a priori state estimate. However, the UKF is less intuitive and computationally heavier and since the computational power is limited during this project the EKF is the chosen method. Other methods include Error-State Kalman and Particle filters but these are not investigated further in this thesis.

### 1.1.1 Similar Work

There has been several theses and reports on the subject of UAV navigation systems. In Magnusson [2013] a full navigation solution is proposed using an EKF. The proposed filter consists of 22 states estimating various parameters, including a quaternion, position, acceleration, sensor biases etc. While this solution presents good results in theory the performance in practice is limited. This was mostly due to the large computational complexity of the filter. Estimating 22 states on a small microprocessor is not possible which points to the conclusion that other solutions where fewer states are estimated should be used. Several problems are discussed throughout the report. One such problem is the accuracy and speed of the GPS used which posed large problems in estimating the states of the filter. This was because the IMU and the GPS provided contradicting data. The report concludes that if a GPS is to be used with the IMU sensors the precision and speed of the GPS has to be high enough to measure possible manoeuvres. Misalignment between the IMU sensors is also discussed as a potential problem and is investigated further in this thesis. The observability of a large filter was also problematic which again points towards a smaller filter to estimate the attitude. The thesis contains well documented sensor information and proposes proper calibration methods that can be used to gain good sensor reliability.

Johansson and Kinner [2011] also discuss a full navigation solution. This thesis presents an EKF solution to the problem and a more intuitive heuristic solution. Both solutions provide good results compared to an AHRS system used during the thesis. The main issues discussed in this thesis are the observability of the filter and the accelerometer bias. The accelerometer bias was not easily estimated thus leading to the accelerometer being less reliable. They also present a 2D calibration of magnetometer as an issue and recommend using a 3D calibration method. Such a method is used in Magnusson [2013] which is also used in this thesis. The solution in Johansson and Kinner [2011] uses Euler angles which can pose problems with singularities in  $\pm 90^\circ$  pitch angles making a quaternion or direction cosine matrix based filter preferred.

These two theses present solutions to both attitude and localisation estimation. However making the attitude estimations more robust and how to remedy the problems posed by using cheap small-scale inertial sensors can be investigated further. The sensitivity of the magnetometer has to be investigated more thoroughly as the magnetometer is easily disturbed by magnetic variations. Magnusson [2013] propose a method to compensate for accelerations by measuring wind speed. This is not possible for all kinds of UAVs such as helicopters. Another approach is to use GPS velocity measurements which can be differentiated to linear accelerations. This method is proposed in Lima and Torres [2012] and is investi-

gated in this thesis.

In conclusion, the main approach with this thesis is to determine a filter which can be implemented on a small microprocessor while still giving robust estimation of the attitude. The filter should work, with minor modifications, on both helicopter and fixed wing UAVs.

## 1.2 Market and Methods

The UAV market is steadily growing. *UAS Europe* is a company located in Linköping, Sweden which develops small-scale fixed wing UAVs with complete autopilot and *Ground Control Station* (GCS) setup. The company is currently investigating the use of small helicopters or multi-rotors. Helicopter UAVs offer more versatility as they allow hovering but lack the range of a fixed wing air craft.



**Figure 1.1:** The Spy Owl 200 fixed wing UAV.

The UAV market is expanding and has evolved steadily during the past years. Earlier the UAVs have mostly been used for military operations but has during later years seen more and more use in civil areas. The UAVs can be used for activities which would be time consuming or dangerous for humans to perform, and are in most cases cheaper than using manned flight to do trivial tasks. The areas where usage of UAVs are applicable include for example industrial security and agricultural oversight.

There are several companies across the globe producing the kind of navigation systems involved in this thesis. Two major companies are:

- Advanced Navigation
- Honeywell Inc.

Both of these manufacturers produce and sell complete navigation systems in various forms. The applications vary from systems for flight, underwater and automotive applications. While these areas are different in a lot of ways the methods to navigate are often similar but with other kinds of sensor equipment.

Some of the flight navigation solutions use the same kind of setup used during this thesis utilising magnetometers, accelerometers and gyroscopes which is

called *inertial navigation* and are often aided by GPS to determine attitude and localisation. Other applications utilise carrier phase measurements from multiple GPS receivers to determine attitude as in Baroni and Koiti Kuga [2012]. This sort of arrangement can be used if the aircraft on which the navigation system is placed is large enough to get different time of arrivals at the different receivers and can hence not be used on small-scale aircrafts due to lacking precision of GPS. Cheap or older GPS modules often have low update frequencies and precisions which make these sort of solutions less useful. However, due to the accuracy of GPS receivers having been significantly improved during the last couple of years this method has been increasingly popular especially for larger aircrafts. The GPS approach is often preferred as magnetometers are easily disturbed and accelerometers being unreliable during accelerated motions. Solutions where the GPS and the inertial sensors are tightly coupled are also frequent.

This leads to the conclusion that the multiple GPS approach will continue to grow in usage. The inertial sensor solutions will still be of big importance since GPS signals are not always available or in some cases lack proper precision. The inertial sensors are also cheap which is why they are frequently used.

Other solutions which are discussed in literature use camera sensors to augment the attitude estimation as in Sazdovski et al. [2010]. With good visibility and knowledge of the area of use this is an effective way to accurately determine the orientation. These solutions offer high precision but are more troublesome to implement performance wise as most imaging applications require a lot of processing capability to be viable in real time applications. These sort of methods are widely studied at the moment, especially for applications where precise attitude estimates with small errors are needed. UAV applications typically do not need this extreme precision which makes the vision based approaches less applicable due to microprocessors often lacking the computational power required.

## 1.3 Motivation

The purpose of this Master's thesis is to evaluate an extended Kalman filter for attitude estimation using inertial sensors on a small-scale UAV. Such an attitude estimation system is often called *Attitude-Heading Reference System* (AHRS) and is used to supply a control unit with sufficient information to enable proper flight control. An inertial AHRS system typically relies on comparing two reference vectors i.e. the gravity vector and the north vector with data from inertial sensors. The angular rate gyros can be used to update the orientation of the aircraft and the drift due to bias can be compensated for by comparison with the known reference vectors. Such a system of high reliability is needed in almost all flight systems but even more so in automated flight.

The EKF was first implemented in Matlab<sup>TM</sup> to investigate the performance of the filter offline and was later implemented in c on the autopilot *EasyPilot 3.0* which is developed by *UAS Europe*.

The autopilot already has a method of determining the attitude, described in section 1.4, which the solution in this thesis is compared to. The *EasyPilot 3.0* autopilot is shown in Figure 1.2.



**Figure 1.2:** The EasyPilot 3.0 autopilot.

*UAS Europe* is interested in an approach which is viable for both fixed wing and helicopter UAVs. The differences in performance between fixed wing air plane and helicopter attitude estimation can vary which makes the evaluation on both kinds of systems important, but during this thesis the filter is only evaluated on a fixed wing UAV.

## 1.4 Previous Solution

The current AHRS solution available on the EasyPilot 3.0 is covered to give insight to what the implemented filter is compared to in Chapter 7. The current method uses an *Explicit Complementary filter* (ECF) and the reference vectors of gravity and the 2D projection of the north vector to compensate for the bias of the gyroscopes. This solution was implemented in Veibäck [2010]. The main advantages with this solution is that a complementary filter is cheap computationally and it is robust. The complementary filter works by combining low-pass filtered input from the accelerometer and magnetometer projected to the gravity plane with high-pass filtered input from the gyroscopes. It is able to provide a good estimate of the attitude in most cases however it is not an optimal estimate meaning that a better one might be possible. The problems with the solution are mostly during straight accelerations such as take-off and landing where the estimated attitude is erroneous. This is dangerous seeing as these are the most crucial moments of flight but overall the current solution performs well. Gyroscope calibration is also important for this solution to work as it does not estimate the gyroscope biases. This also means that drifting estimates might occur after longer time periods.

In this project the attitude is instead determined using an EKF with focus on functionality under suboptimal conditions. Especially the cases of bad magnetometer readings due to disturbances and during accelerated motions. This is also

discussed in Veibäck [2010] where airspeed measurements are used to estimate centrifugal force which increases the performance in long coordinated turns.

The focus on suboptimal conditions raises demands on accuracy and calibration of the available sensors as well as different means to model or measure accelerations and disturbances.

# 2

---

## Coordinate Systems

Reference frames are used in order to relate inputs from the different sensors to the orientation of the UAV. The following coordinate systems are commonly used in different aerial applications.

- Geodetic Frame
- Earth-Centred-Earth-Fixed Frame
- North-East-Down frame
- Body Frame

The North-East-Down frame and the Body frame are relevant in this thesis as the goal is to estimate the *quaternion* or *Tait-Bryant* angles which describe the relationship between these two frames. IMU sensors typically give their measurements in the Body frame and navigation is done in the North-East-Down frame. The other frames are covered in order to give a larger context and the solution is augmented with GPS measurements which are given in the Geodetic frame. The ECEF is used as a middle step between the Geodetic frame and the NED-frame which is described in appendix A.

The North-East-Down frame, Geodetic frame and the Earth-Centred-Earth-Fixed frame are visualised in Figure 2.1 and the relationship between the Navigation frame and the Body frame is visualised in Figure 2.2.

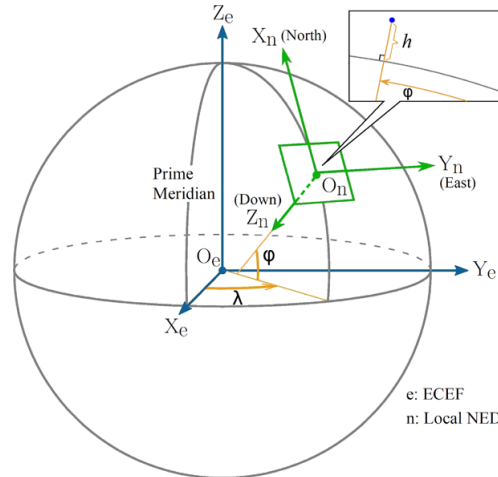


**Figure 2.1:** Image showing the WGS, ECEF and NED reference frames.

## 2.1 Geodetic Frame, WGS

A world geodetic system, WGS is used in order to relate Cartesian coordinates to spherical coordinates given in latitude, longitude and altitude. This frame is most commonly used in GPS applications and models the Earth as a symmetrically round ellipsoid according to minor and major radius  $R_{ea}$ ,  $R_{eb}$  and the flattening  $f$ . The relationship is described in Table 2.1 from Cai et al. [2011].

**Table 2.1:** The parameters for WGS84.

Description	Parameter	Value
Major Radius	$R_{ea}$ [m]	6,378,137
Minor Radius	$R_{eb}$ [m]	$R_{ea}(1-f) = 6,356,752.0$
Flattening	$f$ [-]	1/298.257223563
First Eccentricity	$e$ [-]	$\sqrt{\frac{R_{ea}^2 - R_{eb}^2}{R_{ea}}} = 0.08181919$
Meridian Radius Curvature	$M_e$ [-]	$\frac{R_{ea}(1-e^2)}{(1-e^2 \sin^2 \varphi)^{3/2}}$
Prime Vertical Curvature	$N_e$ [-]	$\frac{R_{ea}}{\sqrt{1-e^2 \sin^2 \varphi}}$

The longitude  $\lambda$  measures angle between the prime meridian and the measured point and ranges between  $-180^\circ$  and  $180^\circ$ . The latitude  $\varphi$  measures angle between the equatorial plane and the normal given by the reference ellipsoid intersecting the measured point. Finally the height  $h$  measures height from sea level determined by the distance to the reference ellipsoid from the measured point.

## 2.2 Earth-Centred-Earth-Fixed Frame, ECEF

The ECEF, *Earth-Centred-Earth-Fixed* reference frame is a Cartesian coordinate system where the origin is placed in the Earth's centre of mass. Since this coordinate system is fixed relative to the Earth the axes also rotate with the earth. The axes are defined as:

**X-axis,  $X_e$ :** Intersects the reference ellipsoid of the earth at  $\lambda = \phi = 0^\circ$ .

**Y-axis,  $Y_e$ :** Orthogonal to  $X_e$  and  $Z_e$  making a right handed coordinate system.

**Z-axis,  $Z_e$ :** Along the spin axis of the Earth pointing towards the north pole.

## 2.3 Norht-East-Down Frame, NED

This is a Cartesian reference frame with an arbitrary chosen origin. The directions are given in North-East-Down headings, which is why this coordinate system is called the NED-frame. The axes are defined, based on the WGS84 reference frame described in Section 2.1, as:

**Origin,  $O_n$ :** Arbitrarily chosen point on the surface of the Earth.

**X-axis,  $X_n$ :** Unit vector pointing towards the geodetic north.

**Y-axis,  $Y_n$ :** Unit vector pointing towards the geodetic east.

**Z-axis,  $Z_n$ :** Unit vector pointing in the direction of the centre of the Earth.

The NED-frame is the most commonly used reference frame when navigating small aircrafts. By noting the takeoff point this frame can be used to describe position, velocity and acceleration with respect to this point. The NED frame can be set to move with the vehicle and is then called *Vehicle-Carried NED*.

## 2.4 Body Frame, $B$

The *Body*, or  $B$ -frame, is centred at the centre of gravity of the vehicle and the axes are aligned with the vehicle. The system is defined as:

**Origin,  $O_b$ :** Positioned at the centre of mass of the vehicle.

**X-axis,  $X_b$ :** Unit vector pointing forward in the symmetric plane of the vehicle.

**Y-axis,  $Y_b$ :** Unit vector pointing starboard (right hand side looking along the X-axis).

**Z-axis,  $Z_b$ :** Unit vector pointing down from the symmetric plane.

Acceleration and velocity in the NED-frame can be described in the B-frame by projection. In avionics the rotations around these axes are called yaw, pitch and roll and the derivatives of these give the rotational speed. These angles describe the orientation of the vehicle with reference to the *Vehicle-Carried NED-frame* which is called the *attitude* of the vehicle.

## 2.5 Rotational Concepts

Rotations are used to transform between different frames. The representation of rotations can be done in a number of ways, two of which are described in this chapter. The most intuitive method to describe attitude is by Euler angles(or Tait-Bryant angles) but this representation has some flaws which is why other forms of representation, i.e. quaternions or direction cosine matrices are used. In this thesis the unit quaternion is used to describe the attitude. The quaternion can then be translated to Euler angles to give a more understandable result.

### 2.5.1 Euler Angles, Tait-Bryant Angles

The most common and simplest form used to describe the rotational state is an Euler angle representation, called Tait-Bryant angles. The orientation of a coordinate system with respect to another coordinate system can be described by three successive Euler rotations according to Cai et al. [2011]. A rotation is represented by a  $3 \times 3$ -matrix and the rotations are done by matrix multiplications and the rotation back is done simply by the transpose of the same  $3 \times 3$ -matrix.

In avionics the Euler angles can be used to describe the relation between the NED-frame and the B-frame according to:

**Yaw,  $\psi$ :** The rotation around the Down-axis in the NED-frame. The heading of the vehicle is the angular difference between the X-axis of the B-frame projected on the plane made up of the North and East axes and the North-axis.

**Pitch,  $\theta$ :** The angular difference between the plane given by the north and east-vector in the NED-frame and the X-axis of the B-frame.

**Roll,  $\phi$ :** The rotation around the x-axis in the *B-frame*.

The three rotation matrices used to describe the rotation between the NED and the B-frame are

$$C_\psi = \begin{bmatrix} \cos(\psi) & \sin(\psi) & 0 \\ -\sin(\psi) & \cos(\psi) & 0 \\ 0 & 0 & 1 \end{bmatrix} \quad (2.1)$$

$$C_\theta = \begin{bmatrix} \cos(\theta) & 0 & -\sin(\theta) \\ 0 & 1 & 0 \\ \sin(\theta) & 0 & \cos(\theta) \end{bmatrix} \quad (2.2)$$

$$C_\phi = \begin{bmatrix} 1 & 0 & 0 \\ 0 & \cos(\phi) & \sin(\phi) \\ 0 & -\sin(\phi) & \cos(\phi) \end{bmatrix}. \quad (2.3)$$

These rotation matrices can be used to form a single rotation matrix by multiplication as

$$C_n^b = C_\phi C_\theta C_\psi \quad (2.4)$$

where the notation  $b$  and  $n$  represents rotation from the NED-frame to the B-frame. The rotation order is from right to left. This means that first the NED-frame is rotated with  $\psi$  which aligns  $X_n$  with the projection of  $X_b$  in the plane composed of the  $X_n$  and  $Y_n$ . This is followed by the rotation of  $\theta$  which aligns the x-axes of the two coordinate systems. Finally the rotation of  $\phi$  aligns the y-axes and the z-axes of the two coordinate systems which means that all axes are aligned. These rotations are visualised in 2.2.

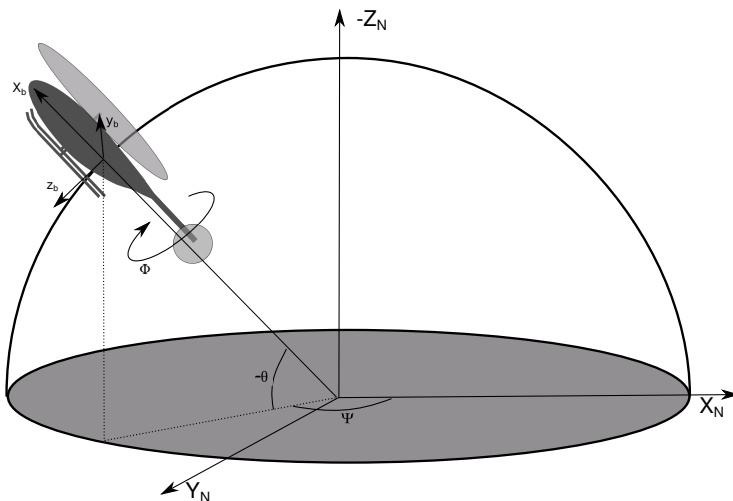


**Figure 2.2:** The relation between the NED-frame and B-frame.

If the matrices are multiplied together the following expression is obtained

$$C_n^b = \begin{bmatrix} \cos(\theta) \cos(\psi) & \cos(\theta) \sin(\psi) & -\sin(\theta) \\ \sin(\phi) \sin(\theta) \cos(\psi) & \sin(\phi) \sin(\theta) \sin(\psi) & \sin(\phi) \cos(\theta) \\ -\cos(\phi) \sin(\psi) & +\cos(\phi) \cos(\psi) & \cos(\phi) \cos(\theta) \\ \cos(\phi) \sin \theta \cos(\psi) & \cos(\phi) \sin(\theta) \sin(\psi) & \cos(\phi) \cos(\theta) \\ +\sin(\phi) \sin(\psi) & -\sin(\phi) \sin(\psi) & \end{bmatrix} \quad (2.5)$$

and since

$$\det(C_n^b) = 1 \quad (2.6)$$

$C_n^b$  is an orthogonal matrix. this means that the inverse can be expressed as a the transpose. The conversion from B-frame to NED-frame can hence be expressed as

$$C_b^n = (C_n^b)^{-1} = (C_n^b)^T \quad (2.7)$$

### Propagation of Euler Angles

The Euler angles are updated through the angular rates  $\omega_x, \omega_y, \omega_z$ . The derivatives  $\dot{\psi}, \dot{\theta}, \dot{\phi}$  through which the Euler angles are updated are derived in Titterton et al. [2004] as

$$\begin{bmatrix} \omega_x \\ \omega_y \\ \omega_z \end{bmatrix} = \begin{bmatrix} \dot{\phi} \\ 0 \\ 0 \end{bmatrix} + C_\phi \begin{bmatrix} 0 \\ \dot{\theta} \\ 0 \end{bmatrix} + C_\phi C_\theta \begin{bmatrix} 0 \\ 0 \\ \dot{\psi} \end{bmatrix}. \quad (2.8)$$

Solving equation (2.8) yields equations

$$\dot{\phi} = (\omega_y \sin \phi + \omega_z \cos \phi) \tan \theta + \omega_x \quad (2.9)$$

$$\dot{\theta} = \omega_y \cos \phi - \omega_z \sin \phi \quad (2.10)$$

$$\dot{\psi} = (\omega_y \sin \phi + \omega_z \cos \phi) \frac{1}{\cos \theta}. \quad (2.11)$$

These equations are straight forward and yields the propagation of the angles. However equation (2.11) is singular at pitch angle  $\theta = \pm 90^\circ$  which limits the use of the Euler representation. That is why an alternative method of representing the attitude is preferred, namely the unit quaternion which is described in the next section.

### 2.5.2 Quaternion Representation

The unit quaternion is an alternative representation of the rotations described in Section 2.5.1. The quaternion representation consists of four complex parameters and is based on the idea that a rotation between two coordinate systems can

be achieved using only one rotation around a vector  $\mu$ . The quaternion representation is widely used in avionics because a rotation is done in one step and the singularity in the Euler representation is bypassed.

The four states that represent the quaternion makes it cheap computationally. A quaternion is denoted  $\mathbf{q}$  and is computed from the vector  $\mu$  and the length of  $\mu$ . This is described in Titterton et al. [2004] as

$$\mathbf{q} = \begin{bmatrix} q_1 \\ q_2 \\ q_3 \\ q_4 \end{bmatrix} = \begin{bmatrix} \cos\left(\frac{\|\mu\|}{2}\right) \\ \frac{\mu_x}{\|\mu\|} \sin\left(\frac{\|\mu\|}{2}\right) \\ \frac{\mu_y}{\|\mu\|} \sin\left(\frac{\|\mu\|}{2}\right) \\ \frac{\mu_z}{\|\mu\|} \sin\left(\frac{\|\mu\|}{2}\right) \end{bmatrix}. \quad (2.12)$$

The magnitude and direction of  $\mu$  is chosen such that a single rotation taking the first reference frame to the second reference frame can be achieved.

The quaternion can also be expressed as a four component complex number with a real component and three imaginary components

$$\mathbf{q} = q_0 + q_1\mathbf{i} + q_2\mathbf{j} + q_3\mathbf{k}. \quad (2.13)$$

According to Titterton et al. [2004] the product of two quaternions,  $\mathbf{q}_1 = [q_0 \quad q_1 \quad q_2 \quad q_3]$  and  $\mathbf{q}_2 = [a \quad b \quad c \quad d]$  can be expressed on matrix form as

$$\mathbf{q}_1 \cdot \mathbf{q}_2 = \begin{bmatrix} q_0 & -q_1 & -q_2 & -q_3 \\ q_1 & q_0 & -q_3 & q_2 \\ q_2 & q_3 & q_0 & -q_1 \\ q_3 & -q_2 & q_1 & q_0 \end{bmatrix} \begin{bmatrix} a \\ b \\ c \\ d \end{bmatrix} \quad (2.14)$$

A quaternion can be used to rotate a vector  $\mathbf{r}_b$  from the b-frame to a vector  $\mathbf{r}_n$  in the NED-frame which is described in Titterton et al. [2004].  $\mathbf{r}_b$  is first expressed as a quaternion where the scalar component is set to zero

$$\mathbf{r}_b = 0 + x\mathbf{i} + y\mathbf{j} + z\mathbf{k}. \quad (2.15)$$

A quaternion  $\mathbf{q}$  can now be used to perform the rotation by quaternion multiplication

$$\mathbf{r}_n = \mathbf{q} \cdot \mathbf{r}_b \cdot \mathbf{q}^*. \quad (2.16)$$

where  $*$  denotes the complex conjugate. This can be expressed on matrix form as

$$\mathbf{r}_n = \begin{bmatrix} 0 & 0 \\ 0 & \mathbf{C} \end{bmatrix} \mathbf{r}_b \quad (2.17)$$

where  $\mathbf{C}$  is derived in Barczyk [2012] as

$$\mathbf{C} = \begin{bmatrix} (q_0^2 + q_1^2 - q_2^2 - q_3^2) & 2(q_1 q_2 - q_0 q_3) & 2(q_1 q_3 + q_0 q_2) \\ 2(q_1 q_2 + q_0 q_3) & (q_0^2 - q_1^2 + q_2^2 - q_3^2) & 2(q_2 q_3 - q_0 q_1) \\ (q_1 q_3 - q_0 q_2) & 2(q_2 q_3 + q_0 q_1) & (q_0^2 - q_1^2 - q_2^2 + q_3^2) \end{bmatrix} \quad (2.18)$$

which rotates from the  $b$ -frame to the NED-frame. This matrix is the same rotation matrix expressed by the Euler angles in (2.5). As this matrix is orthogonal the transpose can be used in order to rotate back to the  $b$ -frame.

### Propagation of Quaternions

In Titterton et al. [2004] angular rates  $\omega$  are used to update the unit quaternion  $\mathbf{q}$  by

$$\dot{\mathbf{q}} = \frac{1}{2} \mathbf{q} \cdot \mathbf{p}_{nb}^b \quad (2.19)$$

where  $\mathbf{p}_{nb}^b$  is defined as:

$$\mathbf{p}_{nb}^b = \begin{bmatrix} 0 \\ \omega_x \\ \omega_y \\ \omega_z \end{bmatrix} \quad (2.20)$$

which can be written on matrix form. This gives

$$\dot{\mathbf{q}} = \frac{1}{2} \begin{bmatrix} q_0 & -q_1 & -q_2 & -q_3 \\ q_1 & q_0 & -q_3 & q_2 \\ q_2 & q_3 & q_0 & -q_1 \\ q_3 & -q_2 & q_1 & q_0 \end{bmatrix} \begin{bmatrix} 0 \\ \omega_x \\ \omega_y \\ \omega_z \end{bmatrix} = \frac{1}{2} \begin{bmatrix} -q_1 & -q_2 & -q_3 \\ q_0 & -q_3 & q_2 \\ q_3 & q_0 & -q_1 \\ -q_2 & q_1 & q_0 \end{bmatrix} \begin{bmatrix} \omega_x \\ \omega_y \\ \omega_z \end{bmatrix}. \quad (2.21)$$

This can be rewritten using the quaternion as a vector and rotation rates describing the rotation matrix

$$\dot{\mathbf{q}} = \frac{1}{2} \begin{bmatrix} 0 & -\omega_x & -\omega_y & -\omega_z \\ \omega_x & 0 & \omega_z & -\omega_y \\ \omega_y & -\omega_z & 0 & \omega_x \\ \omega_z & \omega_y & -\omega_x & 0 \end{bmatrix} \begin{bmatrix} q_1 \\ q_2 \\ q_3 \\ q_4 \end{bmatrix}. \quad (2.22)$$

The equations in equation (2.21) and (2.22) are henceforth used with the nomenclature

$$\dot{\mathbf{q}} = \frac{1}{2} \bar{S}(\mathbf{q}) \boldsymbol{\omega} \quad \dot{\mathbf{q}} = \frac{1}{2} S(\boldsymbol{\omega}) \mathbf{q} \quad (2.23)$$

and are used to update the quaternion with time.

### 2.5.3 Relationship Between Quaternions and Euler Angles

A quaternion can be expressed by Euler angles, which can be derived from the rotation matrix and is described in Titterton et al. [2004], as

$$q_0 = \cos \frac{\phi}{2} \cos \frac{\theta}{2} \cos \frac{\psi}{2} + \sin \frac{\phi}{2} \sin \frac{\theta}{2} \sin \frac{\psi}{2} \quad (2.24)$$

$$q_1 = \sin \frac{\phi}{2} \cos \frac{\theta}{2} \cos \frac{\psi}{2} - \cos \frac{\phi}{2} \sin \frac{\theta}{2} \sin \frac{\psi}{2} \quad (2.25)$$

$$q_2 = \cos \frac{\phi}{2} \sin \frac{\theta}{2} \cos \frac{\psi}{2} + \sin \frac{\phi}{2} \cos \frac{\theta}{2} \sin \frac{\psi}{2} \quad (2.26)$$

$$q_3 = \cos \frac{\phi}{2} \cos \frac{\theta}{2} \sin \frac{\psi}{2} + \sin \frac{\phi}{2} \sin \frac{\theta}{2} \cos \frac{\psi}{2}. \quad (2.27)$$

This can be rewritten to

$$\phi = \arctan \left[ \frac{2(q_2 q_3 + q_0 q_1)}{1 - 2(q_1^2 + q_2^2)} \right] \quad (2.28)$$

$$\theta = \arcsin [2(q_0 q_2 - q_1 q_3)] \quad (2.29)$$

$$\psi = \arctan \left[ \frac{2(q_1 q_2 + q_0 q_3)}{1 - 2(q_2^2 + q_3^2)} \right]. \quad (2.30)$$

In this conversion the non-linearity of the  $\pm 90^\circ$  pitch angle again is a problem and which quadrant of the unit sphere the  $\phi$  and  $\psi$  are in depends on the signs of the nominators and denominators respectively.



# 3

---

## Sensors

This chapter covers the sensors on the *EasyPilot 3.0*. The chapter introduces the sensors and their uses as well as the problems that need to be handled with each sensor. Proposed calibration methods for each sensor are then discussed.

### 3.1 Hardware

The EasyPilot 3.0 is equipped with several sensors using *Micro-Electro-Mechanical Systems*, (MEMS) technology. These are relatively cheap sensors which need analysis and calibration in order to be used with good results. The sensors on the board are as follows.

**3-Axis Gyroscope:** Angular velocity measurements around the B-frame axes.

**3-Axis Accelerometer:** Measures acceleration in x, y, z in body coordinates.

**3-Axis Magnetometer:** Measures magnetic field in x, y, z in body coordinates.

**Pitot Tubes:** Measures dynamic and static pressure.

**GPS:** Measures Longitude, Latitude, Altitude, Heading, Velocity.

The GPS and Pitot Tubes are not as much of importance as the other three when determining attitude. The Pitot Tubes have limited use in attitude estimation on a *Vertical Take-Off and Landing* (VTOL) UAV, and the GPS is mostly used for getting the localisation of the UAV.

The GPS is here also used to augment the attitude estimate by supplying information about the speed which can be differentiated to get an external acceleration reference. This is described later in Chapter 4.

## 3.2 Sensor Performance

The individual performance and issues related to each type of sensor is described later in this chapter. This section describes some related issues which are used to describe performance of multiple types of sensors.

### 3.2.1 Random Walk

A sensor is often subject to different sources of noise. The noise can have different impact on the results obtained from the sensors. This is especially important if the measurements are integrated. Errors from noise will then add up with time, which is called random walk. To measure the magnitude of the impact of the noise the convention *Noise Density* is according to Johansson and Kinner [2011] used. The performance of the gyroscopes are measured in *Angular Rate Density*  $^{\circ}/\sqrt{s}$  or  $^{\circ}/\sqrt{h}$  and accelerometer is measured in  $\mu g/\sqrt{s}$  or  $\mu g/\sqrt{h}$ . They are measures of how much the standard deviation of integrated noise increases with respect to time, which can be expressed as

$$\sigma_{\Theta}(t) = \sigma \cdot \sqrt{\delta t \cdot t} \quad (3.1)$$

where  $\sigma$  is the standard deviation,  $\delta t$  is the sample time,  $t$  is the elapsed time and  $\sigma_{\Theta}(t)$  is the standard deviation at  $t$ . The measure  $\sigma \cdot \sqrt{\delta t}$  is then a measure of how much the integrated signal drifts because of noise. This measure is different depending on the sample time and grows bigger with larger sample time. For large sample times in the measure of a couple of Hz the Allan variance is needed to compute the *Noise Density* which is not described here, see Johansson and Kinner [2011].

### 3.2.2 Inter-Sensor Misalignment

A source of error which is not specific to a single sensor is the misalignment between the different sensors due to placement during manufacturing. This is most important between accelerometer and magnetometer as they are used to correct the attitude determined from the rate gyros. If the coordinate systems between these two sensors are not aligned they will try to correct the orientation in different directions. This can lead to lead to substantial error in estimated attitude if the misalignment is large. There are ways to calibrate these type of errors such as Elkaim [2013], but these calibration methods often depend on precise knowledge of the orientation of the sensor frame which was not available during the time of this thesis. The magnitude of this error is discussed in Section 7.2.5.

## 3.3 Gyroscope

MEMS gyroscopes are frequently used in UAV applications and other strap-down applications because of their low cost and simple use. The 3-axis MEMS gyroscope gives angular rates around the three sensor axes, these axes are fixed to the body which the sensors are attached to and hence give the angular rates around the B-frame axes. These measurements are attained by utilising the Coriolis effect, which states that a frame rotating in a frame with mass  $m$ , angular velocity  $\omega$  and moving at the velocity  $v$  experiences the force

$$F_c = -2m(\omega \times v) \quad (3.2)$$

and the MEMS gyroscopes are composed of vibrating elements that measures this force. Since the gyroscope measure angular rates the current angles can be obtained by integration through equation (2.9), (2.10) and (2.11). This is called the strap-down method and gives a good estimate of the attitude of the rigid body to which the sensor is attached, but only during short periods of time. The main problem with this method is that the gyroscope imposes a bias offset which makes the estimates diverge with time.

### 3.3.1 Performance

As stated earlier a problem with the gyroscopes is the bias which makes the estimates diverge after some time. The scaling factor which scales the raw estimates to angular rates is another issue which has to be addressed. The issues related to the gyroscopes are summed up below.

**Scale factors:** Scale factors are the scaling between raw measurements and angular rates. These are often provided by the manufacturer of the gyroscope but can vary somewhat. This scaling factor is not always constant with respect to time or rotational speed and can hence induce errors in the estimates. This randomness has to be handled by the filter.

**Bias:** There is always a constant bias to the angular rate measurements provided by the gyroscope. Since this bias is integrated the error of the estimates will increase with time according to  $\Theta(t) = \epsilon t$  where  $\epsilon$  is the constant bias. There is also a random bias which is not constant with respect to time.

**Measurement noise:** The gyroscope suffer from measurement noise which has to be analysed.

**Misalignment:** Manufacturing errors might induce errors in the orthogonality of the sensor axes. This means that rotation around one of the sensor axes will affect the output of the other axes as well.

Some performance issues can not be compensated for with the measurement instruments provided during this thesis and is therefore not compensated for.

These errors include sensor specific errors such as resolution, bandwidth, turn-on time and shock resistance. Since the bias of the gyro will be modelled as a state in the filter the change in bias does not have to be compensated for. This will also handle the changes in scale factor. According to Woodman [2007] the random drift errors that appears due to noise can be modelled with a random walk process.

### 3.3.2 Analysis

To measure the performance of the gyroscope data is sampled while the sensor is still and lying flat. These measurements allow the value of the static bias and the variance to be determined. The data is sampled at approximately 90 Hz, due to limits in write speed of the memory card which was used during the logging.

12 seconds of data is presented in Figure 3.1 where the raw data has been converted to radians per second.

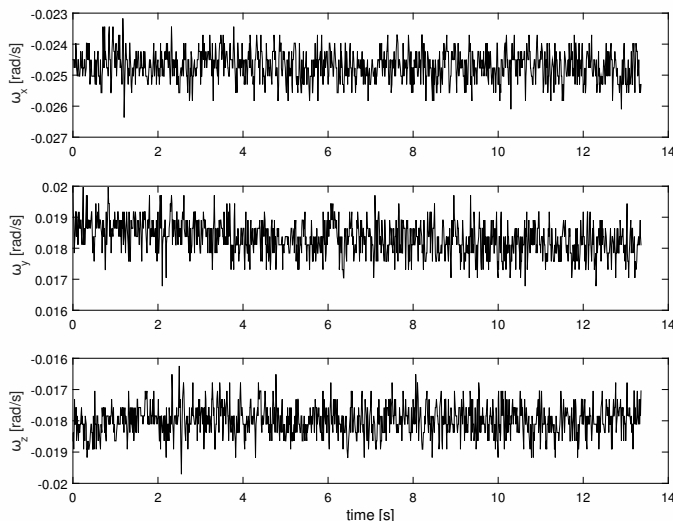


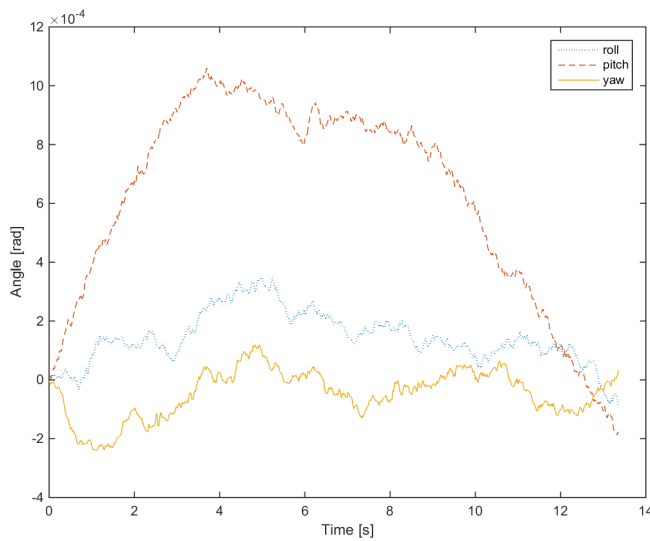
**Figure 3.1:** Static gyroscope measurements..

The constant bias is the mean of this data and the variance is computed. These values are presented in Table 3.1 for each of the sensor axes.

If this data is integrated with compensation of estimated constant bias the results are the random walk sequences presented in Figure 3.2. This random walk is due to integration of noise in the sensor readings. In this case the values for each axis are close to zero in the end but this is rarely the case, see Johansson and Kinner [2011]. This result shows the need to model the noise characteristics of the gyroscope when estimating the attitude.

**Table 3.1:** Bias and variance of static gyro measurements.

Sensor	Bias [rad/s]	Variance [rad <sup>2</sup> /s <sup>2</sup> ]
roll	-0.0247	2.3127e-07
pitch	0.0183	2.9577e-07
yaw	-0.0180	2.4106e-07

**Figure 3.2:** The gyro random walk due to noise.

The random drift due to noise of the sensor is often described in rate noise density [ $^{\circ}/s/\sqrt{Hz}$ ] as described in Section 3.2. This value is provided by the manufacturer but is computed in order to see how well the sensor fares compared to the manufacturer specifications. The calculated rate noise density and the value from the data sheet is presented in Table 3.2. The rate noise density is less than the value

**Table 3.2:** Bias and variance of static gyro measurements.

Sensor	Rate Noise Density [ $^{\circ}/s/\sqrt{Hz}$ ]
Manufacturer	0.005
x-axis	0.0029
y-axis	0.0033
z-axis	0.0030

that the manufacturer has specified which shows that the sensor is functioning properly. This value can vary depending on different resolution settings on the gyroscope as well as how the sensor is mounted on the board and is of course

different for other sensor units.

### 3.3.3 Calibration

The calibration of the gyroscope is not as important as the calibration of the accelerometer and the magnetometer. Most calibration methods need precision reference measurements to present good results and the manufacturer calibration of the gyroscopes proves to be good enough. As was described in Section 3.3.1 the state estimation of the bias term solves many of the errors and makes precise calibration less useful.

This concludes that the manufacturer calibration of the gyroscope should suffice, but means that the calibration of accelerometer and magnetometer needs more focus.

## 3.4 Accelerometer

Accelerometers are common in various automation applications. The accelerometer on the *EasyPilot 3.0* board is a 3-axis MEMS accelerometer. An accelerometer typically consists of a mass anchored in a frame by a spring-damper system. When the frame is set in motion the mass is displaced, this displacement is measured and can be interpreted to acceleration. The accelerometers measure the gravity as well and since the gravity vector is known in NED this information can be used to calculate the roll and pitch angles of the rigid body. In theory the measured acceleration can also be used to estimate both velocity and position by integration, but this is for full inertial navigation, as in Titterton et al. [2004].

### 3.4.1 Performance

Since the accelerometer is of the same technology as the gyroscope the errors which influence the measurements are roughly the same, see Section 3.3. When integrating the accelerometer measurements to determine velocity followed by position the bias error term is integrated meaning that the estimated velocity and position will diverge due to the bias term being added each update. This is not a problem when estimating attitude as the accelerometer bias is not integrated, and hence the small magnitude of the error will not increase with time. It imposes a small error on the estimate but this error is small compared to the external accelerations and gravity measured by the sensor. This is why the bias term of the accelerometer is not modelled in this thesis. It is however calibrated for.

### 3.4.2 Analysis

Accelerometer data from the same test used to analyse the gyroscope is used to analyse the static performance of the accelerometer. The accelerometer will always include the gravity vector which means that the orientation of the board is of important when calculating the bias from the data set. During these measurements the board is lying flat on a bench which should be aligned with the earth. This assumption could be somewhat erroneous since the table or floor is not likely to be completely flat. The data which is sampled at 90 Hz is presented in Figure 3.3

The bias levels of the measurements are calculated as the mean of the measurements. However because of gravity the accelerometer z-axis should measure negative 1G. This means that the bias is the difference between the mean and 1G. This results in the biases and variances according to Table 3.3.

If the accelerometer measurements are integrated and the gravity vector is compensated for, Figure 3.4 is the result. It shows the random walk in velocity estimates due to accelerometer noise. The performance of the accelerometer with respect to noise can be expressed in  $\mu\text{g}/\sqrt{\text{Hz}}$ . This is called the noise density and

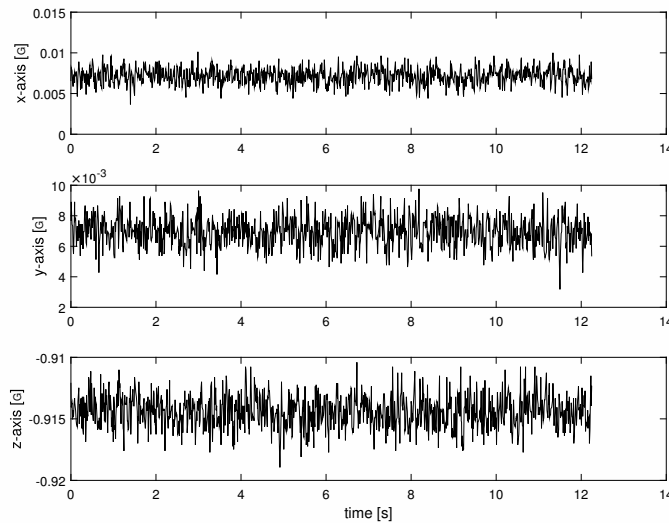


**Figure 3.3:** Static accelerometer measurements

**Table 3.3:** Biases and variances of the accelerometer measurements.

Sensor	Bias [G]	Variance [ $G^2$ ]
x-axis	0.0071	1.0103e-06
y-axis	0.0070	9.3463e-07
z-axis	0.0855	1.7651e-06

the value from the static measurements and the supplied value from the manufacturer is presented in Table 3.4.

**Table 3.4:** Noise density of accelerometer measurements.

Sensor	Noise Density [ $\mu\text{g}/\sqrt{\text{Hz}}$ ]
Manufacturer	400
x-axis	142.7090
y-axis	149.4508
z-axis	272.9140

The calculated values are low which indicates that the sensor is good with respect to noise. As with the gyroscope this value can be different on other sensor units and different setups. A lower sample rate also gives a higher noise density.

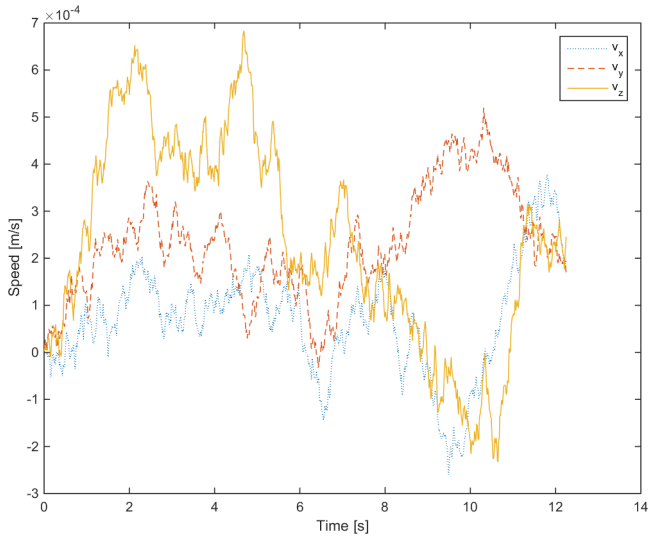


**Figure 3.4:** Accelerometer noise random walk.

### 3.4.3 Calibration

The above measurements in Table 3.3 can be used to compensate for the constant bias. These measurements are however based on scale factors provided by the manufacturer and on the assumption that the misalignment between the accelerometer axes are small. If the scaling is off or the misalignment is in fact large the chosen calibration is not enough. The algorithm presented in this section can then be used to calibrate the sensor. The algorithm is presented in greater detail in Tee et al. [2011] and is outlined here.

#### Error modelling

The sensor readings can be modelled according to the error model

$$v_i = ST^{-1}g_i + b + \epsilon \quad (3.3)$$

where  $v_i$  is raw measurement from the accelerometer at sample  $i$ ,  $S$  contains the scale factors,  $T$  is the misalignment matrix,  $b$  is the constant bias offset on each of the sensor axes and  $\epsilon$  is the noise. The vector  $g_i$  is the gravity vector at sample  $i$ . By assuming that the x-axis of the sensor is aligned with the actual x-axis the misalignment between each axis does not have to be computed which simplifies the expression to a large degree. This is discussed in Skog and Händel [2006]. The number of unknown elements is reduced by three and the final sensor model

is expressed as

$$\begin{bmatrix} v_x \\ v_y \\ v_z \end{bmatrix} = \begin{bmatrix} k_x & 0 & 0 \\ 0 & k_y & 0 \\ 0 & 0 & k_z \end{bmatrix} \begin{bmatrix} 1 & -a_{yz} & a_{zy} \\ 0 & 1 & -a_{zx} \\ 0 & 0 & 1 \end{bmatrix}^{-1} \begin{bmatrix} g_x \\ g_y \\ g_z \end{bmatrix} + \begin{bmatrix} b_x \\ b_y \\ b_z \end{bmatrix}. \quad (3.4)$$

Thus there are 9 unknowns to decide in order to calibrate the sensor. This can be done in numerous ways, the more angles in which the sensor is positioned the better. In Tee et al. [2011] it is concluded that six positions suffice to determine the calibration with good results. Since there where no proper measurement equipment available during this thesis a six position calibration where the gravity vector is aligned with each axis is used.

Equation (3.4) can be rewritten to three separate equations on the form  $y = Ax$  for each of the axes, where the z-axis is easiest to solve followed by the y-axis and lastly the x-axis. This leads to

$$\begin{bmatrix} v_{z_1} \\ v_{z_2} \end{bmatrix} = \begin{bmatrix} 1 & g_{z_1} \\ 1 & g_{z_2} \end{bmatrix} \begin{bmatrix} b_z \\ k_z \end{bmatrix} \quad (3.5)$$

$$\begin{bmatrix} v_{y_1} \\ v_{y_2} \\ v_{y_3} \end{bmatrix} = \begin{bmatrix} 1 & g_{y_1} & g_{z_1} \\ 1 & g_{y_2} & g_{z_2} \\ 1 & g_{y_3} & g_{z_3} \end{bmatrix} \begin{bmatrix} b_y \\ k_y \\ k_{yzx} \end{bmatrix} \quad (3.6)$$

$$\begin{bmatrix} v_{x_1} \\ v_{x_2} \\ v_{x_3} \\ v_{x_4} \end{bmatrix} = \begin{bmatrix} 1 & g_{x_1} & g_{y_1} & -g_{z_1} \\ 1 & g_{x_2} & g_{y_2} & -g_{z_2} \\ 1 & g_{x_3} & g_{y_3} & -g_{z_3} \\ 1 & g_{x_4} & g_{y_4} & -g_{z_4} \end{bmatrix} \begin{bmatrix} b_x \\ k_x \\ k_{xyz} \\ k_{xzy} \end{bmatrix} \quad (3.7)$$

where the numbers 1,2,3 and 4 denotes a configuration in which the sensor is placed and

$$a_{zx} = \frac{k_{yzx}}{k_y} \quad (3.8)$$

$$a_{yz} = \frac{k_{xyz}}{k_x} \quad (3.9)$$

$$a_{zy} = \frac{k_{xzy}}{k_x} + a_{yz}a_{zx}. \quad (3.10)$$

The accelerometer is sampled during ten seconds in static with each of the axes aligned in the direction of gravity, both up and down. The gravity vector can then be expressed as  $\pm 1$  in the direction of each axis and zero in the other two axes, making up six possible gravity configurations. These gravity configurations are matched with the mean of the readings corresponding to the configuration meaning that equations (3.5), (3.6) and (3.7) are solved with different picks of combinations. (3.5) needs two picks, (3.6) needs three picks and (3.7) needs four picks to be solved. With six possible configurations (each axis aligned with positive and negative gravity) the number of possible combinations depending on the number of picks are given in Table 3.5.

The equations (3.5), (3.6) and (3.7) can be solved using the inverse of  $A$  according to  $x = A^{-1}y$  if  $\text{rank}(A) = n$  where  $n$  is the number of unknowns. These are the non-singular matrices in Table 3.5. The equations are solved for each non-singular combination and the mean of the results give the sought variables. With

**Table 3.5:** Number of combinations.

Total\Picks	2	3	4
Combinations	15	20	15
Non-Singular	9	12	12

these variables the conversion to calibrated measurements in G can be solved by

$$a_i = S^{-1} T(v_i - b) \quad (3.11)$$

where  $a_i$  is measured acceleration in G at sample i.

## Results

The calibration method was applied using a workbench vice to keep the autopilot aligned. While this is a crude approach to align the axes in the direction of gravity the method gave reasonable results. The means and standard deviations of the estimated parameters are presented in the Table 3.6.

**Table 3.6:** Estimated parameters.

Parameter	$\mu$	$\sigma$
$b_x$	128.3328	23.2984
$b_y$	55.5807	69.9951
$b_z$	-273.0470	120.1450
$k_x^i$	1.2232e-04	4.3732e-07
$k_y^i$	1.2125e-04	1.1788e-06
$k_z^i$	1.2091e-04	1.9775e-06
$a_{zx}$	0.0108	0.0086
$a_{yz}$	-0.0019	0.0034
$a_{zy}$	0.0164	0.0049

If the sensor is perfect it means that  $a = b = 0$ . Studying Table 3.6 it can be noted that the sensor suffers from both bias and misalignment. The magnitude of the misalignment is however quite small. It can also be noted that both  $a$  and  $b$  have sizable standard deviations which gives large confidence intervals. To increase the precision of the calibration more accurate angle measurements has to be used. If 12 orientations are used instead of the six used here the precision would be better which can be seen in Tee et al. [2011]. Measurements calibrated by this procedure is compared with data that has been converted to G through manufacturer specifications and has been compensated for static bias measured in orientation with z-axis up. This comparison is shown in Figure 3.5 where the autopilot is placed with y-axis down.

The figure shows that the calibrated measurements present improved results, keeping in mind that the accelerometer used only suffers from small errors due

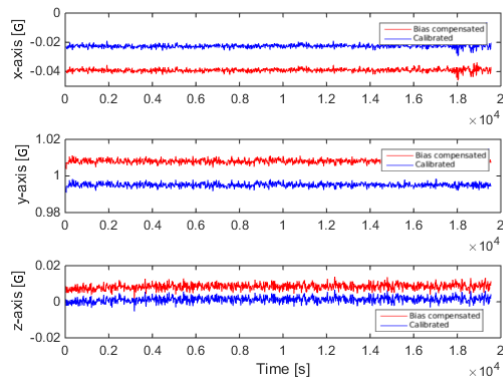


**Figure 3.5:** Comparison between calibration and bias compensation only.

to misalignment. The calibrated measurements are closer to zero for the axes orthogonal to the gravity vector and is closer to 1 G for the axis aligned with the gravity vector. The difference could be larger with another accelerometer where errors due to misalignment or scaling factors are larger.

## 3.5 Magnetometer

The *EasyPilot 3.0* is equipped with a 3-axis magnetometer utilising *Anisotropic Magnetoresistive* (AMR) technology. Magnetometers of the AMR technology are small in size which makes them suitable for UAV applications. The elements in AMR change their resistance, thus their output voltage, depending on the magnetic field applied to the sensor. The sensors are built of four so called wheatstone bridges. When no magnetic field is applied they output half of the input voltage and when a magnetic field is applied the change from the nominal output is proportional to the applied magnetic field. Thus allowing the strength of the magnetic field to be sensed, Renaudin et al. [2010].

The magnetometer acts as a compass by supplying a 3-axis vector pointing in the direction of the geomagnetic field at the position of the sensor. This information is supplied in the sensor coordinates and has to be rotated to the NED-frame to be compared with the geomagnetic field at the position which is a known reference vector. This is illustrated in Figure 3.6 showing the magnetic declination  $\delta$ , which is the angle between the vector pointing to the magnetic north and the vector pointing towards the geodetic north as well as the inclination  $I$  which is the angle between the horizontal field lines of the earth and the magnetic field at the location. It also shows the yaw angle  $\Psi$  as the sensor frame is rotated around the *Down*-axis.

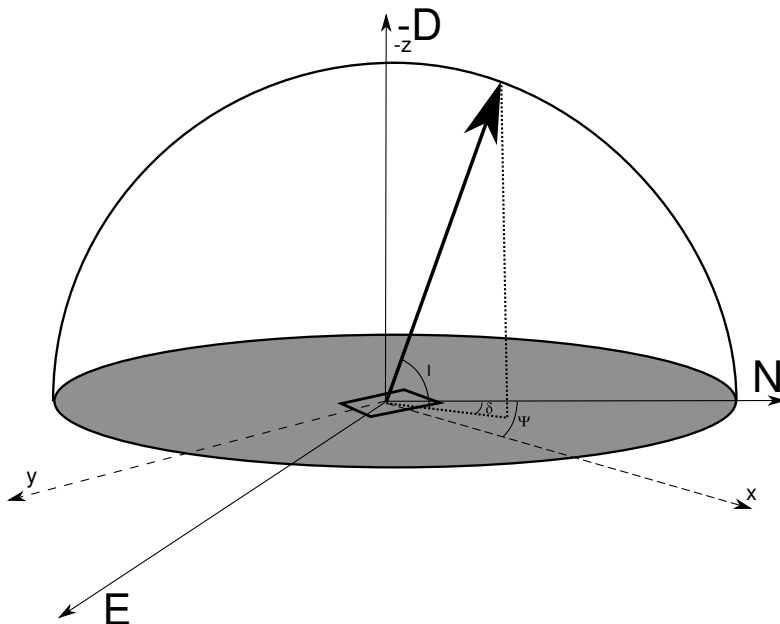


**Figure 3.6:** Magnetic declination and inclination

If the sensor is moved over large distances the information of the local magnetic

field has to be updated in order to utilise the readings given by the magnetometer. The magnetometer offers great potential as comparing the sensed vector with the reference magnetic field vector can be used to get a good estimate of the attitude. Most importantly can this information be used in order to obtain the yaw angle which is where the accelerometer is insufficient. The magnetometer is also undisturbed by external accelerations which affect the accelerometer.

### 3.5.1 Performance

The magnetometer does however have major drawbacks that renders it near useless in some cases and enforces a strong need of calibration. These problems are discussed in this section and a calibration method is presented in 3.5.2.

**Scale Factor Error:** These are errors that corresponds to faults in proportionality of the output of the sensors to the sensed magnetic field.

**Offset Error:** These are constant errors that corresponds to misalignment of the wheatstone bridges that the magnetometer is composed of. Unlike the bias of gyroscopes and accelerometer this offset does not vary with time which makes calibration a proper tool to rid the effects of this error. Often a Helmholtz coil is used for calibration as this gives a good measurement of the applied field according to Renaudin et al. [2010]. This however is not possible during this thesis and the alternative is used. Which is to measure the output at different magnetometer orientations and assume that the applied field is constant which is further discussed in Section 3.5.2.

**Sensitivity Error:** The sensitivity of the AMR elements varies with the amplitude of the measured magnetic field. This results in an error in the scaling of the output from the sensors. This can also be compensated for with calibration and depends on location rather than mounting or the actual sensor. This means that calibration for these types of errors has to be made at each new location. The calibration can be erroneous if the magnetic field magnitude is outside the calibration range.

**Cross Axis Sensitivity:** With time the exposure to a magnetic field the AMR elements get magnetised. This magnetisation is uneven which results in a misalignment of the three magnetometer axes. This can be remedied by demagnifying the AMR elements. According to Renaudin et al. [2010] this is often done by winding a coil along the sensor elements which rectifies the errors.

**Sensor Measurement Noise:** The errors above can all be rectified with proper calibration. The measurements however suffer from measurement noise which cannot be calibrated for. This noise can however be modelled as a stochastic process when using the sensor for attitude estimation.

**Magnetic Field Specific Errors:** The magnetometer is also sensitive to other disturbances of the magnetic field. Ferromagnetic materials and electrical

components near the sensor will generate magnetic fields of their own which disturb the readings of the Earth's magnetic field. These errors are different depending on where the magnetometer is used, i.e. where it is mounted and what the magnetic field angle is at the location of use and are categorised as Hard Iron Errors and Soft Iron Errors.

Hard Iron errors are errors caused by elements which produce a constant magnetic field, such as electrical devices and wires near the sensor. These magnetic field disturbances do not vary with the Earth's magnetic field and are constant depending on the mounting of the sensor.

Soft Iron errors are errors that does vary with the magnitude or orientation of the Earth's magnetic field. The source of these errors are ferro-magnetic materials which possess these attributes. Since these errors vary with the orientation of the magnetic field they are dependant on the orientation of the frame on which the sensor is mounted. This can however also be calibrated for with the proposed calibration algorithm in Section 3.5.2.

### 3.5.2 Calibration

The calibration method is a 3D calibration technique that uses the *least squares* (LS) method and the fact that the sensed magnetic field should always be the same size to fit the sensed data to a unit sphere. This method is presented in Magnusson [2013] and Renaudin et al. [2010]. The calibration provides good results, however it requires the magnetic field to be sensed in all directions in order to adapt the LS to the sphere. This data must be sampled while fitted on the UAV because of the iron errors discussed in the previous section. Such manoeuvring might be troublesome and if that is the case a 2D calibration such as the algorithm presented in Johansson and Kinner [2011] might be used. Here the 3D algorithm is outlined.

#### Error Modelling

The scale factor determines how the input should be scaled in order to generate correct output. This can be modelled with a diagonal matrix as

$$S = \text{diag}(s_x, s_y, s_z) \quad (3.12)$$

The misalignment of the sensors can be modelled by a matrix where the columns give the orientations of the axes. The inverse of this matrix can then be used to correct the non-orthogonality

$$M = N^{-1} = [\epsilon_x \quad \epsilon_y \quad \epsilon_z] \quad (3.13)$$

where  $\epsilon_x$ ,  $\epsilon_y$  and  $\epsilon_z$  vectors of length 3.

The bias can be modelled as an offset

$$\mathbf{b}_m = [b_{m,x} \quad b_{m,y} \quad b_{m,z}]^T. \quad (3.14)$$

The soft iron errors from external magnetic field sources change depending on both the magnitude and the direction of the sensor readings. This error can be modelled by

$$A_{si} = \begin{bmatrix} a_{11} & a_{12} & a_{13} \\ a_{21} & a_{22} & a_{23} \\ a_{31} & a_{32} & a_{33} \end{bmatrix} \quad (3.15)$$

and the hard iron errors are applied as a constant bias

$$b_{hi} = [b_{hi,x} \ b_{hi,y} \ b_{hi,z}]^T. \quad (3.16)$$

The complete model is then summarised by

$$\hat{h} = SM(A_{si}h + b_{hi}) + b_m + \epsilon \quad (3.17)$$

where  $h$  is the sought magnetic field,  $\hat{h}$  is the raw readings from the magnetometer with errors and  $\epsilon$  is noise. This model can be expressed as:

$$\hat{h} = A \cdot h + b + \epsilon \quad (3.18)$$

where

$$A = SMA_{si} \quad b = SMb_{hi} + b_m. \quad (3.19)$$

Since the goal is to remove all errors with the calibration this is a valid expression. Each individual error does not have to be computed which makes calibration of the errors easier.

## Results

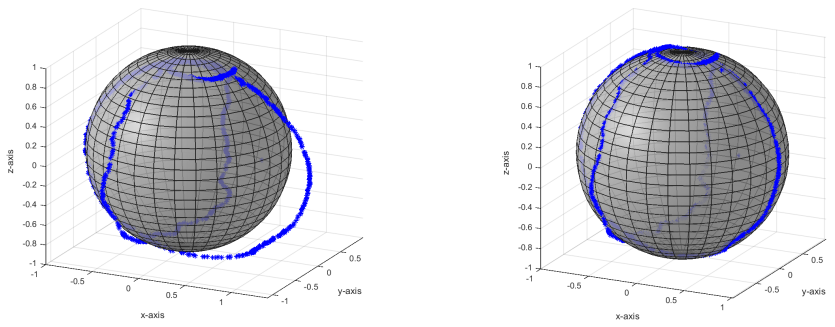
The algorithm uses data sensed in all directions and tries to fit the data to a sphere using LS.

The error model in equation (3.18) can be solved by first rewriting the expression to:

$$h = A^{-1}(\hat{h} - b - \epsilon) \quad (3.20)$$

and then solving it using the LS-method as proposed in Magnusson [2013] which gives the calibration matrix  $A^{-1}$  and the bias term  $b$ .

The calibration gives the results visualised in Figure 3.7b. This figure shows both non-calibrated measurements and calibrated measurements plotted on a unit sphere. The values should be aligned with the sphere if the measurements are correct. The non-calibrated measurements are off in both scaling and offset. The calibration improves the measurements significantly as these are more aligned to the sphere. This result can be improved further if samples are taken in a wider arc such that larger parts of the unit sphere is covered. This makes it easier to fit a LS-estimate to the readings.



(a) Uncalibrated measurements.

(b) Calibrated measurements.

**Figure 3.7:** Images showing uncalibrated and calibrated measurements plotted on a unit sphere.

## 3.6 GPS Module

The GPS on the autopilot is a U-Blox GPS module. In most applications the main purpose of the GPS is to determine position by triangulation but during this thesis it is used in order to get accurate velocity measurements.

As described in Zogg and U-Blox [2009] the GPS uses the *Global Navigation Satellite System*, GNSS to determine the position and speed. The manufacturers often use the *National marine electronics association* (NMEA) protocol to communicate with the satellites. The position is determined by comparing the time differences between messages sent from the satellites. More recent GPS devices such as the one on the *EasyPilot 3.0* features velocity measurements that are determined from Doppler shifts. The Doppler shift depends on how fast the receiver is moving to or from the satellites. The experienced frequency will be shorter if the receiver is moving towards the satellite and larger if the receiver is moving from the satellite, this information can then be used to determine the course and velocity of the receiver. This theory is visualised in Figure 3.8.

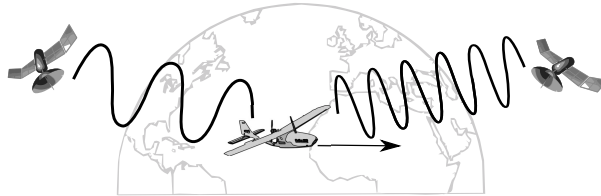


**Figure 3.8:** The Doppler effect between signals from two satellites.

The GPS on the *EasyPilot 3.0* allows velocity measurements with accuracy of up to 0.1m/s and heading precision of 0.5° according to the manufacturer which is a significantly higher accuracy than if the position would have been differentiated to get velocity. The GPS allows position to be determined with an accuracy of ~ 2m which would lead to large errors if differentiated to get velocity.

The U-Blox GPS module supplies velocity measurements in three variables course, horizontal speed and vertical speed. These measurements have to be fitted to the NED axes which is done by

$$v_N = v_h \cos(\delta) \quad (3.21)$$

$$v_E = v_h \sin(\delta) \quad (3.22)$$

$$v_D = -v_v \quad (3.23)$$

where  $\delta$  is the course and  $v_h$  and  $v_v$  are the horizontal and vertical speed respectively.

### 3.6.1 Performance

The GNSS is largely effective at providing highly accurate information about the position and speed of the receiver. The GPS measurements however have some drawbacks which according to Zogg and U-Blox [2009] are

**Satellite Location:** The satellite location is not exact leading to errors in estimated position and velocity.

**Satellite Clocks:** Although the satellites include four atom clocks each the timing is not exact. As an example, a 10ns timer error results in a 3m error according to Zogg and U-Blox [2009].

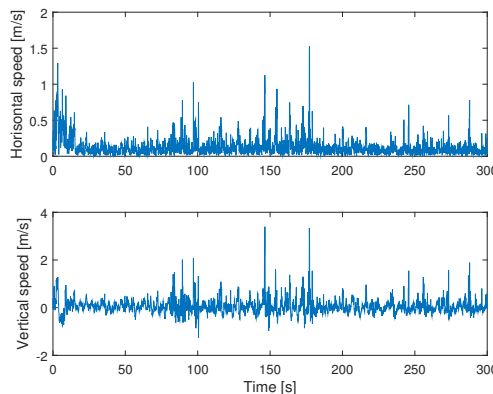
**Multipath:** These are effects related to GPS signals being reflected from the environment, for example buildings, trees and mountains. This is why the GPS precision is better in open terrain or up in the air.

**Atmosphere Errors:** These are errors relating to variations of gas molecule concentration and humidity in the troposphere as well as ionization levels in the ionosphere. These measures vary the speed of light and hence the time of arrival.

**Other Errors:** How the satellites are arranged vary the accuracy of the measurements. Further, the the accuracy can be dependent on receiver functionality, for example time delays and measurement noise can increase the errors.

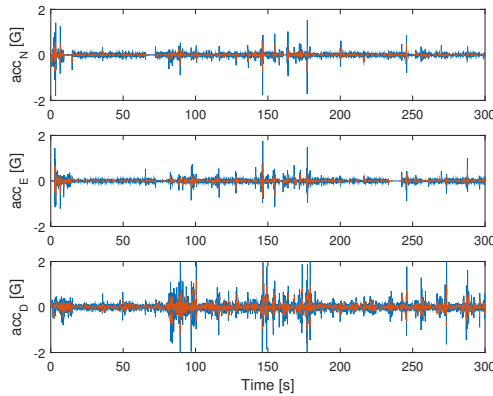
### 3.6.2 Analysis

Figure 3.9 shows 5 minutes of GPS speed measurements when the receiver was placed in stand still on the ground. The measurements were sampled in a cityscape environment which influences the measurements in a negative way.



**Figure 3.9:** GPS measurements during 5 minutes of stand still measurements.

The sampled course and speed readings are translated to velocity measurements in the NED-frame which can in turn be differentiated to get acceleration. The large factor of noise however leads to large errors in estimated acceleration. This can be reprimanded to some degree by low-pass (LP)-filtering the estimate from 10Hz to 5Hz. The estimated acceleration and the LP-filtered estimate based on the data above is presented in Figure 3.10 where the dashed line is the LP-filtered estimate.



**Figure 3.10:** GPS acceleration estimate during stand still measurements.

This concludes that estimated acceleration is quite severely affected by the noise in GPS measurements. The variances of the three axes are presented in Table 3.7. Where the vertical acceleration estimate is clearly less accurate than the horizontal accelerations. With the accuracy in mind the GPS acceleration should not be used when a good estimate of the gravity is possible without compensating for external accelerations. In other words, when the magnitude of the accelerometer is close to gravity, the GPS acceleration should not be used. There are some problems with this approach as some manoeuvres can result in measurements of 1G even though an external acceleration is applied, for example when descending and turning at the same time. This can be solved by checking so that the GPS acceleration is approximately 0 as well. The effects of the GPS noise are incorporated in the model leading to less trust in measurements when GPS measurements has to be used. Trusting the measurements less compensates for the lack of accuracy in these measurements.

**Table 3.7:** Variance of estimated acceleration.

acc <sub>N</sub> , [G]	acc <sub>E</sub> , [G]	acc <sub>D</sub> , [G]
0.0043	0.0050	0.0305

The accuracy of the GPS velocity measurements is drastically improved when in flight and in motion. In motion the Doppler shift difference is clearer allowing

higher accuracy and in flight the multipath errors are largely avoided.

## 3.7 Sensor-Platform Performance

The sensor performance while fitted on a UAV is largely different from the performance on test bench. The sensor readings are both affected by engine vibrations and due to magnetic disturbances from electrical circuits and chords.

### 3.7.1 Vibrations

The accelerometer detects all kinds of accelerations and this includes vibrations from the engine. In order for the vibrations to affect the filter estimates to a degree as small as possible the measurements have to be anti-alias filtered through a moving average filter. The averaging is done so that the sample rate of the accelerometer is lowered to approximately 5Hz. This allows movements of the UAV to be detected while still removing large part of the engine noise. The method is visualised in Figure 3.11 where disturbances from the engine of the *Spy Owl 100* fixed wing are evaluated. Engine thrust is applied three times and sensor data is logged. The gray lines are the raw measurements and the blue lines are the filtered measurements. This however means that the accelerometer can only be used in the EKF measurement update with 5Hz intervals which should be enough to correct for the offset gyro bias errors might cause.

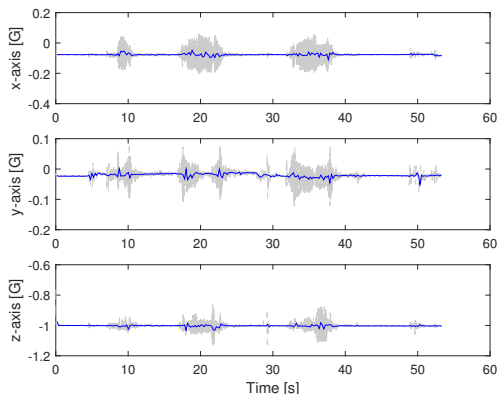


**Figure 3.11:** LP-filtered and raw accelerometer measurements.

There are other filter alternatives which might perform better, especially with respect to stopband attenuation and roll-off. However, the moving average filter is superior when it comes to execution speed, see Smith [1997]. Filters like Gaussian and Blackman are slow because they use convolutions and other recursive filters often require more multiplications. Due to the computational simplicity of the moving average filter it is the chosen method.

### 3.7.2 Magnetic Disturbances

If cables are placed badly or are drawn improperly the magnetometer will be disturbed by electrical currents such as engine thrust. To test the effects on the *Spy Owl 100* the same data as during the vibrations test in Figure 3.11 is used. The magnetometer sensor readings can be seen in Figure 3.12. The test shows that with proper placement of magnetometer, circuits and cables the disturbance effects from the engine can be minimal. This does not mean that this always is the case as magnetometer can be disturbed if the power cable is moved during motion or due to other magnetic field error sources.

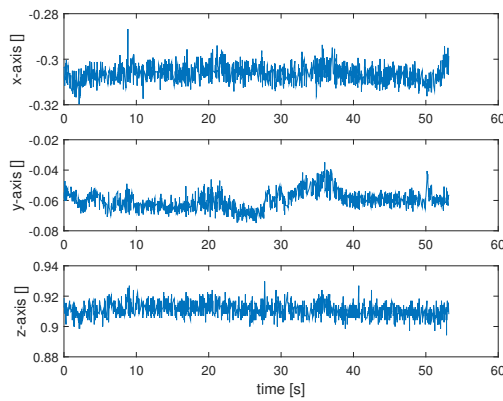


**Figure 3.12:** magnetometer during engine on/off test.

# 4

---

## Sensor Models

This section covers the different sensor models that will be used in the implemented EKF. The states to be estimated is the quaternions representing the attitude and the gyro bias. The states are given on matrix form

$$\begin{bmatrix} q \\ b^g \end{bmatrix} = \begin{bmatrix} q_0 \\ q_1 \\ q_2 \\ q_3 \\ b_0^g \\ b_1^g \\ b_2^g \end{bmatrix}. \quad (4.1)$$

### 4.1 System Dynamics

The proposed model uses gyroscope angular velocity measurements to describe the quaternion dynamics as

$$\dot{q} = \frac{1}{2} S(\omega)q. \quad (4.2)$$

This is a state model with non-linear input from the gyroscope. The gyroscope bias is incorporated in the measurements and has to be compensated for. The model is then expressed as

$$\dot{q} = \frac{1}{2} S(\omega - b^\omega)q \quad (4.3)$$

which as described in Törnqvist [2006] can be written as

$$\frac{1}{2} S(\omega - b^\omega)q = \frac{1}{2} \left( S(\omega)q + \bar{S}(q)b^\omega \right). \quad (4.4)$$

$S(\omega)$  and  $\bar{S}(q)$  are described in Section 2.5.2.

The bias is incorporated in the model. The bias is constant with respect to time and is varying only as a random walk sequence depending on the noise. The complete dynamics model is therefore

$$\dot{q} = \frac{1}{2}S(\omega - b^\omega) \quad (4.5)$$

$$\dot{b}^\omega = 0 + v \quad (4.6)$$

where  $v$  is noise. This is the so called *strap down* approach. The accelerometer and magnetometer are then used as measurements to compensate for the drift from the gyro bias error.

## 4.2 Accelerometer

The accelerometer measurements are used in the measurement model. It uses the fact that the gravity vector in the NED-frame is known. This allows rotation of the gravity vector to the B-frame to be compared with the measured acceleration. The measurement model is described as follows.

$$y_h^a = C_b^n(a - g) + b^a + e^a \quad (4.7)$$

$C_b^n$  is the rotation from the NED to the B-frame which is the transpose of equation (2.18),  $b^a$  is the bias and  $e^a$  is a noise process. The noise process can be modelled as a white noise process. This equation can be approximated with  $a \approx 0$ . This makes this model valid only if the external acceleration  $a$  is small enough. Otherwise a method to measure or model the acceleration has to be used. In fixed wing air plane applications pitot tubes can be used to measure air speed which can be used to get acceleration by derivative, see Magnusson [2013]. GPS measurements can be used to give velocity which can be used to get acceleration in the same manner which is described in Lima and Torres [2012]. This works for longer accelerated manoeuvres but raises high demands on GPS accuracy. Another approach is to model the external acceleration as a low-pass filtered Gauss Markov process as in Lee et al. [2012]. The approach used in here is the GPS approach which is described in Section 4.5.2. Since the bias is not incorporated in the system model the measurement model has to be adjusted. The adjusted measurement is

$$\tilde{y}_h^a = y^a - b^a \quad (4.8)$$

and the final model, assuming that  $a \approx 0$ , is

$$\tilde{y}_h^a = C_b^n(-g) + e^a \quad (4.9)$$

where  $g = [0 \ 0 \ 1]^T$ . If the external acceleration is measured and is non-zero the measurement model is

$$\tilde{y}_h^a = C_b^n(a_e - g) + e^a \quad (4.10)$$

where  $a_e$  is the external acceleration.

## 4.3 Magnetometer

the magnetometer is modelled in the same way as the accelerometer. It uses the fact that the magnetic field at a given position in the NED is known. This information can be rotated to the B frame to be compared with the measured field. The measurement model can then be expressed as

$$y_h^m = C_b^n B^N + e^m. \quad (4.11)$$

$C_b^n$  again is the rotation from NED to B and  $B^N$  is the magnetic field in the NED-frame. The magnetic field is given by  $B^N = [15.7235 \ 1.2643 \ 48.4887]$  in Linköping, Sweden where the thesis is done.

## 4.4 Linearization and Discretization

Both system dynamics and the measurement models are non-linear. To use these models in the EKF they have to be linearised.

The system dynamics also have to be discretized. The discretization is done with the Euler forward method. This is expressed as

$$x(t+T) = A^{(t)}x(t) \quad (4.12)$$

where  $A^{(t)} = I + A_c^{(t)}T$ , see Gustafsson et al. [2011], where  $A_c$  may vary with time. This is a fairly simple approximation but should suffice for this application. After each update, both measurement and system dynamics, the quaternion has to be normalised to keep the unit length. This done according to

$$q = \frac{q}{\|q\|} \quad (4.13)$$

### 4.4.1 System Dynamics

The linearised and discretized system dynamics is given as follows

$$x_{k+1} = \left( I + \begin{bmatrix} \frac{T}{2}S(\omega_k - b_k^g) & -\frac{T}{2}\bar{S}(q_k) \\ 0 & 0 \end{bmatrix} \right) x_k + \begin{bmatrix} \frac{T^3}{4}\bar{S}(q_k) \\ TI \end{bmatrix} v_k \quad (4.14)$$

where  $T$  is the sample time and  $v$  is the noise. The noise from the bias affects the dynamics of the quaternions due to the fact that the biases are used in the update of the quaternions.

### 4.4.2 Measurement Model

The accelerometer and magnetometer measurements have to be linearised in order to update the EKF appropriately.

## Accelerometer

According to Törnqvist [2006] the adjusted accelerometer measurement model is given by

$$y^a = h_a(q_t) + e_t^a. \quad (4.15)$$

This measurement is linearised by

$$y_t^a = h_a(\hat{q}_{t|t-1}) + e_t^a \approx h_a(\hat{q}_{t|t-1}) + H_t^a(q_t - \hat{q}_{t|t-1}) + e_t^a \quad (4.16)$$

where  $H_{a,t}$  is the Jacobian of the measurement model. This is derived as

$$H_t^a = \frac{\partial h^a(q_t)}{\partial q_t} \Big|_{\hat{q}_{t|t-1}} \approx \left\{ a \approx \begin{bmatrix} 0 & 0 & g \end{bmatrix}^T \right\} \approx \quad (4.17)$$

$$\frac{\partial}{\partial q} \begin{bmatrix} 2(q_1 q_3 - q_0 q_2) \\ 2(q_2 q_3 + q_0 q_1) \\ q_0^2 - q_1^2 - q_2^2 + q_3^2 \end{bmatrix} = 2g \begin{bmatrix} -q_2 & q_3 & -q_0 & q_1 \\ q_1 & q_0 & q_3 & q_2 \\ q_0 & -q_1 & -q_2 & q_3 \end{bmatrix}. \quad (4.18)$$

If the external acceleration on the body is estimated the Jacobian is expressed as

$$H_t^a = 2 \cdot \begin{bmatrix} [q_0 \ q_3 \ -q_2] a_e^n & [q_1 \ q_2 \ q_3] a_e^n & [-q_2 \ q_1 \ -q_0] a_e^n & [-q_3 \ q_0 \ q_1] a_e^n \\ [-q_3 \ q_0 \ q_1] a_e^n & [q_2 \ -q_1 \ q_0] a_e^n & [q_1 \ q_2 \ q_3] a_e^n & [-q_0 \ -q_3 \ q_2] a_e^n \\ [q_2 \ -q_1 \ q_0] a_e^n & [q_3 \ -q_0 \ -q_1] a_e^n & [q_0 \ q_3 \ -q_2] a_e^n & [q_1 \ q_2 \ q_3] a_e^n \end{bmatrix}. \quad (4.19)$$

## Magnetometer

The magnetometer measurements are linearised in the same manner as the accelerometer measurements according to Törnqvist [2006]. The magnetometer measurements are hence linearised by

$$y_t^m = h_m(\hat{q}_{t|t-1}) + e_t^m \approx h_m(\hat{q}_{t|t-1}) + H_t^m(q_t - \hat{q}_{t|t-1}) + e_t^m \quad (4.20)$$

where  $H_t^m$  again is the Jacobian. This Jacobian is computed the same way as the accelerometer Jacobian but the magnetic field vector  $B^n = [n_x \ n_y \ n_z]^T$  in the NED-frame is used instead of the gravity vector. The Jacobian is expressed as equation (4.21).

$$H_t^m = 2 \cdot \begin{bmatrix} [q_0 \ q_3 \ -q_2] B^n & [q_1 \ q_2 \ q_3] B^n & [-q_2 \ q_1 \ -q_0] B^n & [-q_3 \ q_0 \ q_1] B^n \\ [-q_3 \ q_0 \ q_1] B^n & [q_2 \ -q_1 \ q_0] B^n & [q_1 \ q_2 \ q_3] B^n & [-q_0 \ -q_3 \ q_2] B^n \\ [q_2 \ -q_1 \ q_0] B^n & [q_3 \ -q_0 \ -q_1] B^n & [q_0 \ q_3 \ -q_2] B^n & [q_1 \ q_2 \ q_3] B^n \end{bmatrix}. \quad (4.21)$$

## 4.5 Problems

This section describes some problems with the proposed model and how they are to be solved.

### 4.5.1 Magnetometer Sensitivity

As discussed in Section 3.5 the magnetometer is sensitive to a large variety of error sources. This makes the magnetometer model valid only when the measurements are inside a specific working range. This can be discovered by checking the norm of the measurements at each sample. If the measurements are calibrated the norm of the measurements should be approximately one. If the measurements diverge above a threshold value  $\epsilon_{mag}$  the measurements cannot be trusted.

An additional test is to check the inclination angle. If the inclination angle differs from the magnetic reference inclination angle the measurement is seen as invalid. This method depends on the estimated attitude due to the fact that the measurement needs to be rotated to NED to determine the inclination angle. This means that this method can not be used if the attitude estimation is erroneous which is hard to determine.

Since the magnetometer is easily distorted only yaw should be updated since this is where the accelerometer is not sufficient. By doing this a disturbed magnetic field should only affect the magnetic heading of the UAV and not the entire attitude. This is achieved using a modification of the method proposed in Madwick [2010]. The method uses the approach to modify the magnetic reference field to have the same inclination as the measurements. This makes the measurements correct only the offset in measured declination and hence only the yaw offset is compensated for. The method in Madwick [2010] uses magnetic reference calculated from the measurements rotated to the B-frame according to

$$y_{NED} = (C_n^b)^T y_B. \quad (4.22)$$

The reference is then updated to

$$B^n = \begin{bmatrix} \sqrt{y_{NED,x}^2 + y_{NED,y}^2} \\ 0 \\ y_{NED,z} \end{bmatrix} \quad (4.23)$$

which has the same inclination as the measurements. While this is a good approach it uses the simplification that the magnetic declination is  $0^\circ$ . A better approach is to use the known magnetic reference field and set the z-axis reference to 0. The NED-frame measurements in (4.22) is also modified by setting the z-value to 0 and is then rotated back to the B-frame to be used as measurement. This way the magnetic declination is used and the inclination is the same for both measurements and reference field.

Both the modified reference field and measurements are then normalised before being used in the measurement update. The method is summed up as

$$\mathbf{y}_{B,mod} = C_n^b \begin{bmatrix} \mathbf{y}_{NED,x} \\ \mathbf{y}_{NED,y} \\ 0 \end{bmatrix} \quad (4.24)$$

$$\mathbf{B}_{mod}^n = \begin{bmatrix} \mathbf{B}_x^n \\ \mathbf{B}_y^n \\ 0 \end{bmatrix} \quad (4.25)$$

$$\mathbf{y}_{B,mod} = \frac{\mathbf{y}_{B,mod}}{\|\mathbf{y}_{B,mod}\|} \quad \mathbf{B}_{mod}^n = \frac{\mathbf{B}_{mod}^n}{\|\mathbf{B}_{mod}^n\|} \quad (4.26)$$

This method is successful if the pitch and roll estimates are fairly accurate, however if these estimates are off the wrong quaternions will be affected. The method also simplifies the linearization matrix which is good concerning computational aspects.

### 4.5.2 Accelerated Motion

The hard part with using accelerometers for attitude determination is the fact that when the rigid body is accelerated the accelerometer no longer only measures gravity but also measures the external acceleration. This can as in the case with the magnetometer also be discovered by checking the norm of the calibrated measurements and see if this value diverges more than  $\epsilon_{acc}$  from 1. This is not always true however as some manoeuvres can give an accelerometer output close to 1 even though the motion is completely different. These manoeuvres include spherical motions along a certain sphere. This is however quite unlikely but to make the demand safer the accelerometer measurements have to be inside  $[1 - \epsilon_{acc}, 1 + \epsilon_{acc}]$  for some time for the measurements to be valid. This method was used in Rehbinder and Hu [2004].

In Lima and Torres [2012] a method to use GPS velocity measurements is proposed. This method both use differentiated velocity measurements and velocity measurements together with angular rates in order to determine the external acceleration. The acceleration can then be expressed as

$$\mathbf{a}_e = \mathbf{g} + \dot{\mathbf{V}}_{GPS} + \boldsymbol{\omega} \times \mathbf{V}_{GPS} \quad (4.27)$$

where  $\mathbf{a}_e$  is the external acceleration,  $\mathbf{g}$  is the gravity vector,  $\mathbf{V}_{GPS}$  are velocity measurements from the GPS and  $\boldsymbol{\omega}$  is gyro angular rate measurements. All measurements are transferred to the NED frame. This method should be able to estimate both linear and centripetal accelerations but demands a high precision GPS to produce good results. The differentiation to get acceleration from velocity measurements is done simply by

$$\dot{\mathbf{V}}_{GPS}^k = \frac{\mathbf{V}_{GPS}^k - \mathbf{V}_{GPS}^{k-1}}{T_{GPS}} \quad (4.28)$$

where  $T_{GPS}$  is the GPS sample time. A modified approach is to use only the differentiated measurements as

$$\mathbf{a}_e = \mathbf{g} + \dot{\mathbf{V}}_{GPS} \quad (4.29)$$

## 4.6 Magnetic Modelling

An approach to modelling the magnetic disturbances affecting the magnetometer is evaluated. The approach is described in Roetenberg et al. [2005]. The method models the magnetic disturbance of each sensor axis as a state

$$\mathbf{d}_m = \begin{bmatrix} d_{m,x} \\ d_{m,y} \\ d_{m,z} \end{bmatrix}. \quad (4.30)$$

The magnetic disturbance is then modelled as a Gauss-Markov process according to

$$d_{m,t} = c_d \cdot d_{m,t-1} + v_d \quad (4.31)$$

where  $c_d$  is a constant between 0 and 1 and  $v_d$  is Gaussian noise. The noise has standard deviation  $\sigma_d$ .

The standard deviation of the disturbance noise  $\sigma_d$  is updated through measurements from the magnetometer. The update depends on changes in magnetic inclination and measurement norm. If the the norm  $\|m_t\| = 1$  and the inclination is equal to the local magnetic inclination  $\varphi_m = 72^\circ$  then  $\sigma_d = 0$ . The standard deviation is then updated through

$$\sigma_d = \sigma_m \left| \|m_t\| - \|m_{t-1}\| \right| + \sigma_{\varphi_m} \left| \varphi_{m,t} - \varphi_{m,t-1} \right| \quad (4.32)$$

so the uncertainty grows larger with changing magnetic field and should then be able to estimate erroneous magnetic measurements.  $\sigma_m$  and  $\sigma_{\varphi_m}$  are tuning factors that determine the noise from the changes.

The drawbacks of this method are that the filter states are increased by three as well as it might be hard to determine the error in inclination from actual change in magnetic field. The results using this method is presented in Section 7.5.



# 5

---

## Extended Kalman Filter

The extended Kalman filter is implemented according to the algorithms which are derived in Gustafsson [2012] and they are summarised in this chapter.

### 5.1 Theory

The use of an ordinary Kalman filter denoted KF is to estimate the states in a linear state space model according to

$$x_{k+1} = F_k + G_k v_k \quad (5.1)$$

$$y_k = H_k x_k + e_k \quad (5.2)$$

$$\mathbb{E}(x_0) = \hat{x}_{1|0} \quad (5.3)$$

$$\text{Cov}(x_0) = P_{1|0} \quad (5.4)$$

which can be extended to use inputs  $u$ , such as information from the user or controller. This can be thrust or turning controls for example. The initial state is without any observations propagated by

$$\hat{x}_{k|0} = F_k \hat{x}_{k-1|0} \quad (5.5)$$

$$P_{k|0} = F_k P_{k-1|0} F_k^T + G_k Q_k G_k^T. \quad (5.6)$$

The KF finds the optimal linear filter to an observation  $y_k$  as

$$\hat{x}_{k+1|k} = M_k \hat{x}_{k|k-1} + L_k y_k \quad (5.7)$$

$$P_{k+1|k} = M_k P_{k|k-1} M_k^T + L_k R_k L_k^T. \quad (5.8)$$

The best linear unbiased filter is according to Gustafsson [2012]) given by Algorithm 1. The prediction is unbiased if  $M_k = F - L_k H$  which gives that equation (5.7) can be written as

$$\hat{x}_{k+1|k} = F\hat{x}_{k|k-1} + L_k(y_k - H\hat{x}_{k|k-1}). \quad (5.9)$$

---

**Algorithm 1** The Kalman filter

---

**1. Measurement update:**

Compute Kalman gain and update:

$$\begin{aligned} K_k &= P_{k|k-1}H_k^T(H_kP_{k|k-1}H_k^T + R_k)^{-1} \\ \hat{x}_{k|k} &= \hat{x}_{k|k-1} + K_k(y_k - H_k\hat{x}_{k|k-1} - D_k u_k) \\ P_{k|k} &= P_{k|k-1} - K_kH_kP_{k|k-1} \end{aligned}$$

**2. Time update:**

$$\begin{aligned} \hat{x}_{k+1|k} &= F_k\hat{x}_{k|k} \\ P_{k+1|k} &= F_kP_{k|k}F_k^T + G_kQ_kG_k^T \end{aligned}$$


---

## 5.2 The Extended Kalman Filter

Since the states which are to be predicted are non-linear the KF has to be extended into an Extended Kalman filter, EKF. The non-linearity of states and measurements can be described as:

$$x_{k+1} = f(x_k, v_k) \quad (5.10)$$

$$y_k = h(x_k, e_k) \quad (5.11)$$

The EKF works in the same way as the ordinary KF. The difference is that the nonlinearities has to be handled by linearization. The EKF linearises the nonlinear function  $z = g(x)$  with a first order Taylor expansion according to:

$$z = g(x) = g(\hat{x}) + g'(\hat{x})(x - \hat{x}) + r(x; \hat{x}, g''(\xi)) \quad (5.12)$$

where  $g'(x)$  denotes the Jacobian of the function  $g(x)$  and  $r$  is the rest term. This implementation is applicable as long as the rest term is small in terms of estimation error and degree of non-linearity of  $g$ . The linear states are handled exactly the same as in the linear case as the linearization does not alter these states. A second order EKF tries to estimate the rest term  $r$ . The EKF algorithm is presented in Algorithm 2. The main issue with the EKF is that the optimality the ordinary KF presents is no longer guaranteed. The observability or convergence of the filter is not guaranteed either. But if the non-linearities are small the EKF presents a near optimal estimation.

---

**Algorithm 2** The Extended Kalman filter

---

**1. Measurement update:**

Linearize measurements:

$$H = \left. \frac{\delta h(x,u)}{\delta x} \right|_{\hat{x}_{k|k-1}}$$

Compute Kalman gain and update:

$$K_k = P_{k|k-1} H_k^T (H_k P_{k|k-1} H_k^T + R_k)^{-1}$$

$$\hat{x}_{k|k} = \hat{x}_{k|k-1} + K_k (y_k - H_k \hat{x}_{k|k-1} - D_k u_k)$$

$$P_{k|k} = P_{k|k-1} - K_k H_k P_{k|k-1}$$

**2. Time update:**

Linearise dynamics:

$$F = \left. \frac{\delta f(x,u)}{\delta x} \right|_{\hat{x}_{k|k}}$$

Update:

$$\hat{x}_{k+1|k} = f(\hat{x}_{k|k}, u_k)$$

$$P_{k+1|k} = F_k P_{k|k} F_k^T + G_k Q_k G_k^T$$


---

## 5.3 Iterated Kalman

The filters above requires inversions of big matrices since the matrices are as big as the dimension of the measurements. These inversions are costly and should, if they can, be avoided. This is where the iterated KF can be used. The iterated KF allows each individual measurement to be fused separately making the inversions less costly. This also allows measurement updates as soon as there is new data to use instead of waiting for the slower sample rates to determine the processing speed. The iterated Kalman filter is given in Algorithm 3.

This algorithm can also be fused with the EKF to an iterated EKF. This is done by inserting the linearization steps from algorithm 2.

## 5.4 Observability

The observability of a discrete system is given by the observability matrix. The system is said to be observable if the observability matrix is of full rank, see

---

**Algorithm 3** The Iterated Kalman filter
 

---

**1. Measurement update:**

For measurement  $i=1:m$

Compute Kalman gain and update:

$$\begin{aligned} K_k^i &= P_{k|k-1}^{i-1} (H^i)^T (H^i P_k^{i-1} (H_k^i)^T + R^i)^{-1} \\ \hat{x}_k^i &= \hat{x}_k^{i-1} + K_k^i (y_k^i - H^i \hat{x}_k^{i-1} - D^i u_k) \\ P_k^i &= P_k^{i-1} - K_k^i H^i P_k^{i-1} \end{aligned}$$

Finally:

$$\begin{aligned} \hat{x}_{k|k} &= \hat{x}_k^m \\ P_{k|k} &= P_k^m \end{aligned}$$

**2. Time update:**

Update:

$$\begin{aligned} \hat{x}_{k+1|k} &= f(\hat{x}_{k|k}, u_k) \\ P_{k+1|k} &= F_k P_{k|k} F_k^T + G_k Q_k G_k^T \end{aligned}$$


---

Gustafsson [2012].

$$\mathcal{O}_{n_x} = \begin{bmatrix} H \\ HF \\ HF^2 \\ \vdots \\ HF^{n_x-1} \end{bmatrix} \quad (5.13)$$

For stochastic dynamic systems the observability grammian can be used instead, which is in Bageshwari et al. [2009] expressed as:

$$\mathcal{O}_N^T \mathcal{O}_N = H_0^T H_0 + \sum_{k=1}^N \Phi_{k-1,0}^T H_k^T H_k \Phi_{k-1,0} \quad (5.14)$$

The observability is given by the rank of the grammian. If  $\mathcal{O}_N^T \mathcal{O}_N$  has full rank the system is observable. This test does not depend on the number of measurements but depends on the dimensions of the state vector. The observability ensures that all states in the state vector can be influenced by the measurements.

#### 5.4.1 Monitoring EKF Performance

There is no guarantee that the EKF will converge according to Gustafsson [2012]. The lack of this property is troublesome since this makes tuning of the filter more important than if convergence is guaranteed. Big initial covariances can easily make the filter diverge which raises demands on a proper initialisation procedure.

There are also methods to adapt the filter with time so that convergence is nearly guaranteed which are not covered in this thesis.

A way to monitor the filter divergence is needed in order to determine how the filter is performing. If the filter does diverge the current AHRS should be used instead. The current solution proved to be robust and always converge. It might give estimates that are off, but this is better than diverging estimates. First outlier detection is applied to remove measurements that would impair the estimation more than they would help. The outlier test statistic is described in Gustafsson [2012] as

$$T(y_k) = (y_k - h(\hat{x}_{k|k-1}))^T (H_k^T P_{k|k-1} H_k + R_k)^{-1} (y_k - h(\hat{x}_{k|k-1})) \quad (5.15)$$

and  $T(y_k)$  can then be used to detect whether the measurement is an inlier or outlier.

The filter divergence can be measured by the sum of outlier test statistics also given in Gustafsson [2012] as

$$T(y_{1:N}) = \sum_{k=1}^N (y_k - h(\hat{x}_{k|k-1}))^T (H_k^T P_{k|k-1} H_k + R_k)^{-1} (y_k - h(\hat{x}_{k|k-1})) \quad (5.16)$$

where  $h$  is the non-linear measurement model and the test is given by

$$\left( \frac{T(y_{1:N})}{N_{n_y}} - 1 \right) \sqrt{N_{n_y}/2} > \phi_a \quad (5.17)$$

where  $\phi_a$  is given by the standard Gaussian error function. Using all samples over time is inappropriate which is why an exponential window is used. This is expressed in Gustafsson [2012] as

$$T(y_{1:k}) = \lambda T(y_{1:k-1}) + \frac{1-\lambda}{n_y} \cdot (y_k - h(\hat{x}_{k|k-1}))^T (H_k^T P_{k|k-1} H_k + R_k)^{-1} (y_k - h(\hat{x}_{k|k-1})) \quad (5.18)$$

where  $\lambda$  is the forgetting factor  $0 << \lambda < 1$ . The filter is diverging if  $T >> 1$  where an appropriate threshold has to be chosen to determine divergence.



# 6

---

## Implementation

In this chapter the implemented solution is described. The hardware implemented on and the concerns associated with the implementation are described.

### 6.1 EasyPilot 3.0

The board on which the implementation is done is called EasyPilot 3.0 and is an autopilot. The board consists of two processors and the sensors described in Section 3.1. One processor contains the AHRS. The other processor handles control of the UAV depending on the input from the AHRS. Both processors are small ARM processors. The processing speed is 168 MHz which raises high demands on the speed of the implemented algorithm.

### 6.2 Computational Complexity

To simplify matrix inversions an iterated EKF described in Algorithms 3 and 2 is used. This drastically reduces the computational complexity of the inversions and makes the EKF able to handle sensor measurements arriving at different speeds which is the case with the magnetometer and the accelerometer.

The computational complexity of the implemented filter is however still a problem. The matrix operation  $\mathbf{F}\mathbf{P}\mathbf{F}^T$ , where all matrices are  $7 \times 7$ , takes on average about 0.8767ms to evaluate. This sort of matrix operations is what makes the implementation rather slow and on the ARM processor the filter can operate at an average frequency of 70 Hz. This is also the main reason for implementing a 7-state filter instead of a larger which can model more states such as accelerations

and magnetic disturbances. The speed of the filter is sufficient for all manoeuvres but a faster implementation is always better as more recent sensor data can be processed if the filter is faster making the filter more up to date. The original AHRS runs at a faster frequency due to the computational simplicity of the explicit complementary filter.

### 6.3 Initialisation

In order to avoid choosing a large  $P_0$  matrix which could lead to divergence an initiation procedure is used. The gyro bias states are initialised with the pre-calculated static biases which should give a reasonably good initial guess. The initial attitude is on the other hand obtained using only magnetometer readings to determine the yaw angle which can be converted to quaternions using equation (2.24). This method can easily be derived from Figure 3.6. It relies on the fact that the sensors are approximately horizontal to the ground during the initialization, meaning that the roll and pitch angles are approximately  $0^\circ$ . The mean of the first 50 magnetometer readings are used to calculate the initial yaw by

$$\Psi = \text{atan}2(-\text{mag}_{meas,x}, \text{mag}_{meas,y}) - \text{Inclination} \quad (6.1)$$

where  $\text{Inclination} = \text{atan}2(-\text{mag}_{ref,N}, \text{mag}_{ref,E})$ .

With the proposed initialisation procedure the initial state values should be a good starting point of the estimations and hence smaller  $P_0$  values can be chosen.

### 6.4 Pre-processing

The magnetometer, accelerometer and gyro use the calibration methods presented in Chapter 3. The gyroscopes use manufacturer settings as scale factor and is corrected using estimated bias. The accelerometer model uses measurements in g and the magnetometer model uses normalised measurements which give the direction of the magnetic field and not the strength.

The accelerometer measurements are LP-filtered to approximately 5 Hz in order to avoid noise from engine vibrations. Further, this is appropriate as the measurement update is not done with each accelerometer measurement which increases the speed of the algorithm. The GPS measurements are also LP-filtered in order to provide measurements with the same sample rate as the accelerometer.

Each magnetometer measurement is rotated to the NED frame and the Z-value is removed, the measurement is then rotated back and normalised. While this takes some computation it must be done in order for magnetic disturbances to affect only the yaw estimate.

# 7

---

## Results

In this chapter the results of the thesis are presented.

### 7.1 Tests

Data was logged on a test bench and in flight to determine the overall performance of the filter in a Matlab™ environment and is compared with the previous ECF solution. The filter was later implemented in c and the performance was tested with similar tests.

**Static Tests:** To determine the stability over longer periods of time static tests were done. These tests show how the filter performs with respect to sensor bias and other errors which grow with time.

**Acceleration Tests:** In order to determine the performance of the filter during accelerations both ground tests and in-air tests were evaluated.

**Magnetic Disturbance Tests:** The EKF performance is hindered by magnetic disturbances due to the sensitivity of the magnetometer. These tests will measure how much the performance is altered and how the disturbances are managed.

**Normal flight:** The EKF is evaluated when performing standard flight manoeuvres in order to determine the overall functionality of the filter.

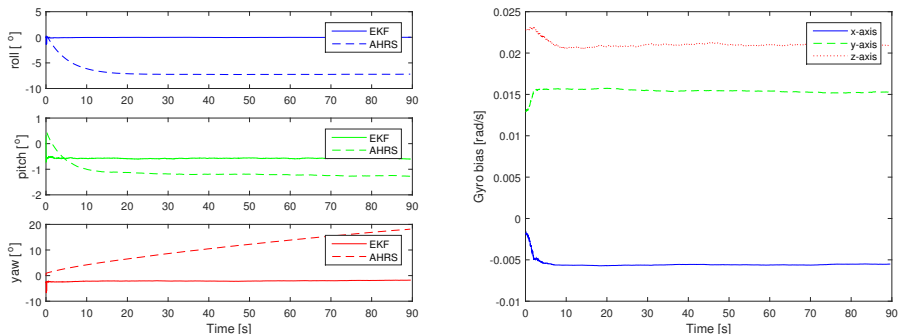
**Observability Tests:** During simple tests on test bench the observability is evaluated in Matlab™. This is to ensure that all states are influenced by the measurement and dynamic models.

## 7.2 Test bench

The sensors are mounted horizontally on a board which is used outside in order to use undisturbed magnetometer measurements. Both static tests and some tests with simple moves are done in order to determine if there are any conceptual flaws and to tune parameters of the filter.

### 7.2.1 Static tests

Figure 7.1a shows the filter during static measurements compared with the current AHRS and figure 7.1b shows the estimated gyro biases during the same period. These figures indicate that the EKF with seven states performs quite well in static behaviours. The estimations does not drift after the initial transient which also is the case for the logged AHRS for roll and pitch. The yaw angle does however drift for the AHRS. This is probably due to improper calibration which is of more importance for the ECF than for the EKF, and because the ECF does not use the magnetometer much. The biases are approximately constant after the initial transient which indicates that the true values have been found.



(a) Estimated Euler angles during static test. (b) Estimated gyro biases during static test.

**Figure 7.1:** Static test bench test.

### 7.2.2 Magnetic Disturbance Tests

To determine the magnitude of the error caused by magnetic disturbances a magnetic disturbance was induced during test bench measurements in order to configure appropriate means of compensating for the effect of the unwanted disturbances. Figure 7.2 shows the norm of the magnetic measurements when a disturbance is induced. The magnetic disturbance is caused by holding a piece of iron close to the magnetometer which perturbs the magnetic field.

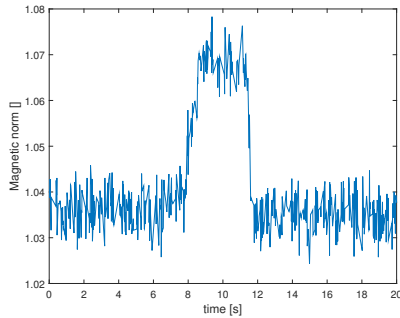


**Figure 7.2:** Norm of magnetic measurements during disturbance.

Figure 7.3 shows the estimated attitude based on the measurements. When the disturbance is induced the estimated attitude is severely erroneous, with an error of  $15^\circ$  in yaw and both pitch and roll angles which diverge from their nominal values.

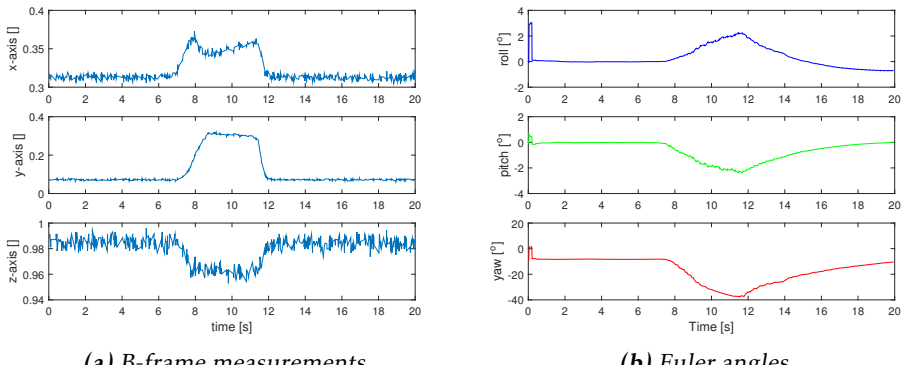


**Figure 7.3:** Magnetic measurements and attitude during magnetic disturbance.

The first thing that can be noted is that the disturbance affects all three angle estimates. The method to update solely yaw from magnetometer measurements in 4.5.1 is applied. The result is seen in figure 7.4. The method is successful in the sense that only the yaw is distorted by the disturbance.

Both the norm of the measurements and the inclination angle are checked to determine if the measurement is erroneous. An error of 5% is allowed in both norm and inclination. The interval in which the norm is allowed can not be chosen smaller as it is not possible to calibrate the magnetometer with good enough precision and the error interval of the inclination cannot be smaller because of errors in estimations. These error levels are tuning factors which are quite hard to chose

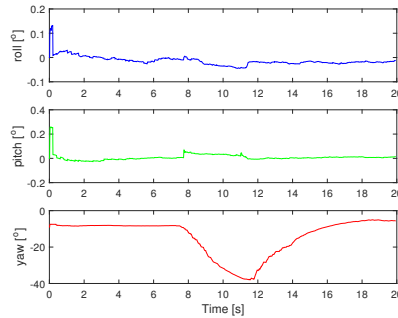


**Figure 7.4:** Euler angles when only yaw is updated by magnetometer.

because an error interval which is too small will cut too much information and a large interval uses disturbed data. The result when the method is used is presented in figure 7.5 which clearly shows an improvement. The angle error due to the magnetic disturbance is only about  $2^\circ$  in yaw angle.

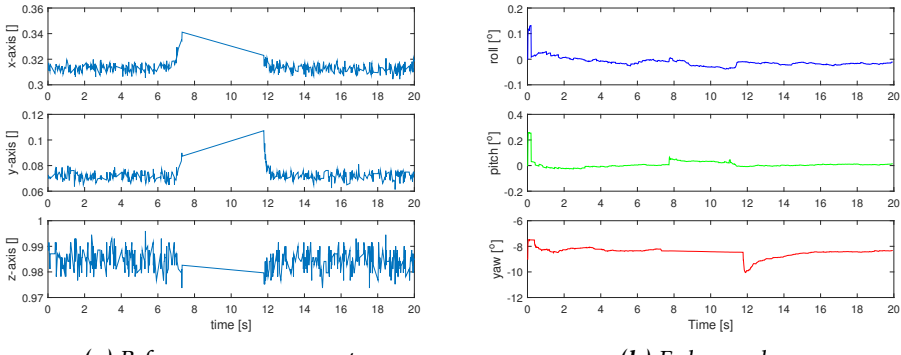


**Figure 7.5:** Compensated measurements and attitude during magnetic disturbance.

### 7.2.3 Acceleration Tests

The effects from external accelerations are tested by generating such accelerations by car. Sensor data was logged on a track that was first ordinary road, then four laps in a round-about and then back the same road stopping in the original direction. Figure 7.6 shows the route. Pitch and roll are approximately constant with some small changes due to road bumpiness. Since magnetometer measurements were not available in the car the starting heading was pre-determined. The yaw angle should be near aligned at the beginning and end of the test. Two methods

to compensate for accelerations are used. The first method is to throw away measurements with a magnitude outside of  $|g \pm \epsilon|$  and the second method uses GPS velocity measurements to calculate the acceleration. The results using method 1 are shown in figure 7.7 and the results from method 2 in figure 7.8.

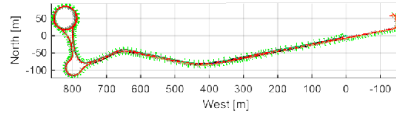
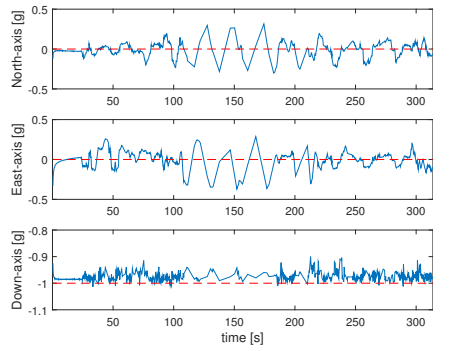
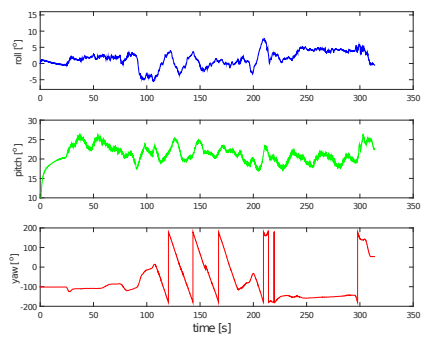


**Figure 7.6:** Route during car test.

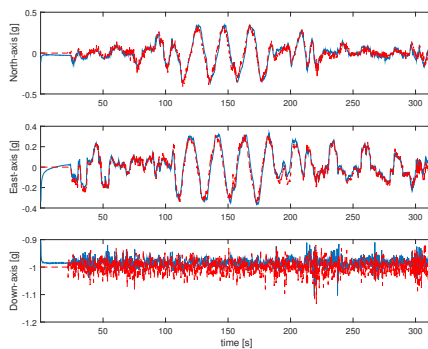


**(a)** Acceleration in NED frame.

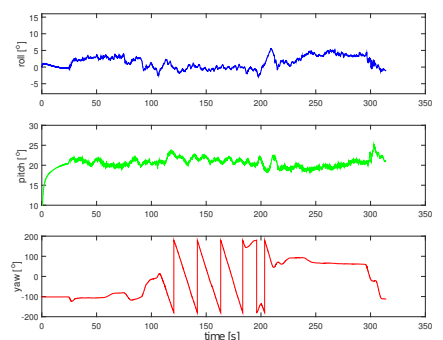


**(b)** Euler angles.

**Figure 7.7:** Car test results with no acceleration compensation.



**(a)** Acceleration in NED frame.



**(b)** Euler angles.

**Figure 7.8:** Car test results with GPS acceleration compensation.

As can be seen by comparing Figures 7.7b and 7.8b method 2 produces smaller errors in pitch and roll due to the external accelerations. The first method is also unable to estimate a correct yaw angle and drifts due to gyro bias errors. This results in a final yaw angle which diverge from the original value. Figure 7.8a shows that the GPS method is successful in estimating an approximate acceleration which corresponds to the acceleration measured by the accelerometer. This method is also able to estimate yaw when accelerating. This means that if the heading is approximately correct at the starting point the method will be able to correct small gyro bias errors. In constant velocity this is however not the case as the acceleration vector is parallel to the yaw-rotation.

## 7.2.4 Dynamic Tests

Figures 7.9a and 7.9b shows the estimated attitude during simple manoeuvres. The sensor board is moved three times in roll, then three times in yaw and finally three times in pitch direction. The reason that there is some interference is that the ground where the test was performed was not absolutely flat. Figure 7.10 shows the gyro biases during the same period. What can be said is that the attitudes are estimated roughly as they should. However since there is no ground truth available no major conclusions can be drawn. The strap-down method should give a good reference since it should only diverge towards the end when the addition of the bias offset has grown too large. This seems to be the case when comparing the strap-down method and the EKF in Figure 7.9b seeing as the strap down method drifts towards the end. The EKF and the ECF seem to perform with roughly the same result. The ECF shows some difference in pitch and roll due to different calibration. This also makes the yaw angle drift after some time which is not the case with the EKF.

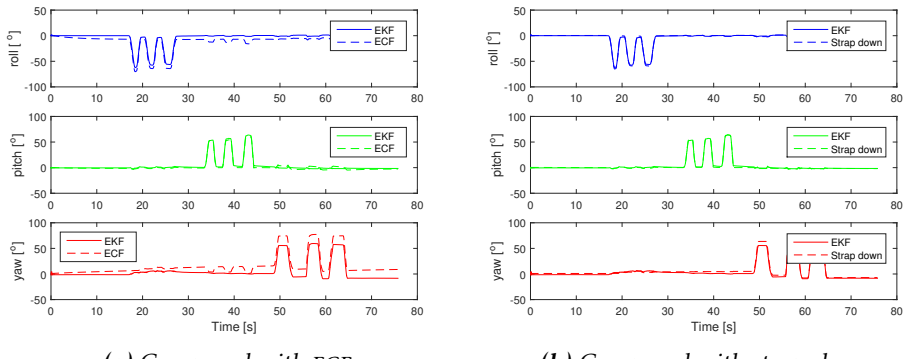


**Figure 7.9:** Estimated Euler angles during dynamics test

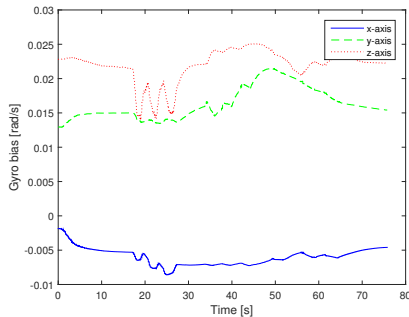


**Figure 7.10:** Estimated gyro biases during dynamics test.

## Observability

The observability of the filter is measured through the observability gramian described in 5.4. The rank of the gramian remains at full rank during the whole dynamic sequence seen in Figures 7.9 and 7.10 which indicates that observability is achieved throughout the measurements.

### 7.2.5 Sensor Calibration and Misalignment

To determine the performance of the calibration a simple test is performed where the magnetometer covariance is set to a small number and the accelerometer covariance is set to a larger number. This means that the magnetometer is trusted to a greater extent than the accelerometer. The accelerometer and magnetometer measurements are then rotated to the NED frame and is then compared to the reference value used in the measurement update. If both sensors are perfectly calibrated both measurements should converge towards the reference value.

The board is moved to about 45° roll where it is held for 30 seconds and is then moved back. The move is shown in figure 7.11 and the accelerometer and magnetic measurements are shown in figures 7.12 and 7.13. As can be seen the accelerometer and magnetometer are fairly close to their reference values when rotated to the NED frame. However, after the move the accelerometer is no longer aligned with the reference value due to the fact that the magnetometer is trusted more. The reason for the difference is likely due to the inter-sensor misalignment errors discussed in chapter 3. This difference is still not a major issue as the error is relatively small. This effect can also be a result of inexact calibration of the sensors. To achieve better calibration other measurement equipment which was not available during this thesis is needed.

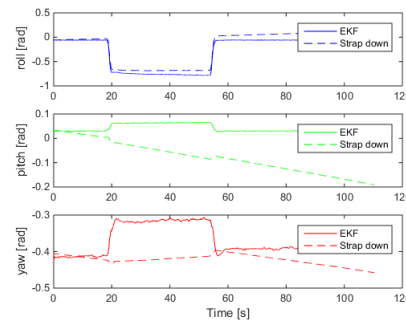


**Figure 7.11:** Estimated Euler angles during misalignment test.

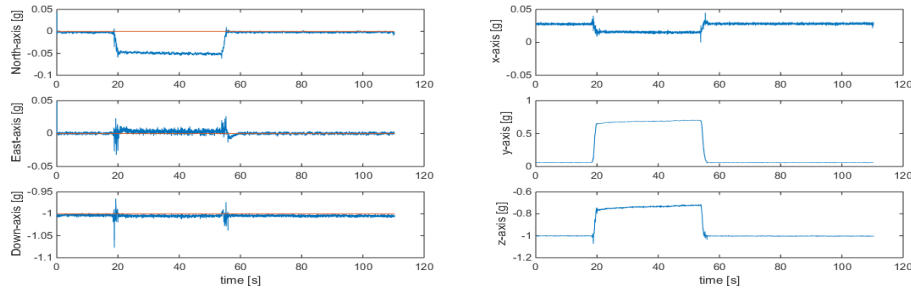


**Figure 7.12:** Accelerometer measurements during misalignment test.

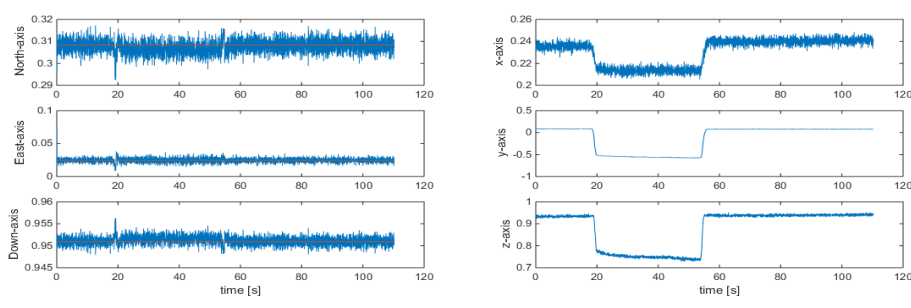


**Figure 7.13:** Magnetometer measurements during misalignment test.

## 7.3 Flight Tests

Flights was performed where sensor data was logged and the filter was evaluated in Matlab™. Flights were logged with the fixed wing aircraft, Spy Owl 100. The 7-state EKF performs well compared to the complementary filter implementation and handles accelerations without diverging. The attitude during the entire flight can be seen in figure 7.14a and the gyro biases during the flight is seen in Figure 7.14b.

The yaw angle looks to deviate from the complementary filter which drifts with time due to offsets in calibration. However the yaw curves fit each other well disregarding the offset between the two methods.

In pitch and roll the two systems perform roughly the same. Figure 7.15 shows the attitude during a roll manoeuvre and Figure 7.16 is during accelerations up and down. The red, green and blue arrows are the body frame axes in respective frame and the black arrow is the course given by the GPS. If the acceleration during descent and ascent in Figure 7.16 are studied it seems that they perform a little bit different. This is largely due to the compensation of external accelerations being different which is discussed in Section 7.3.1.

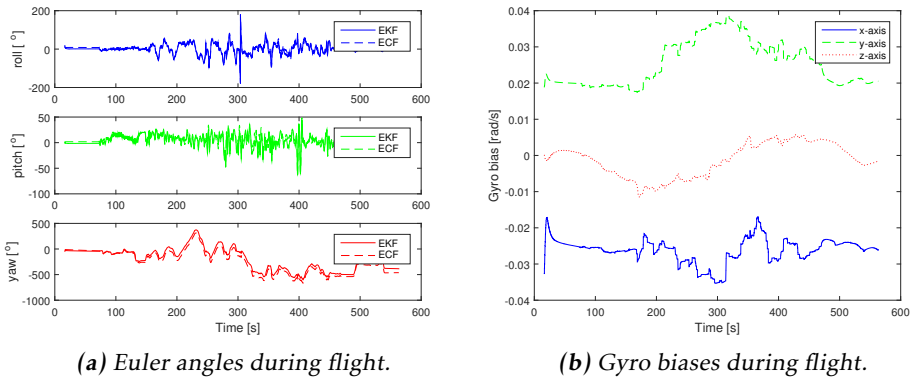
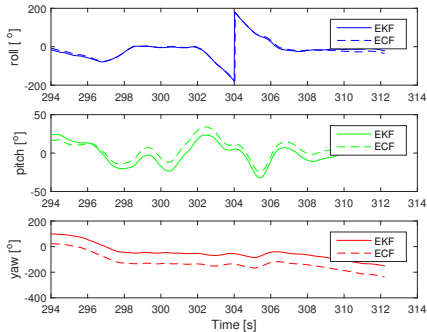
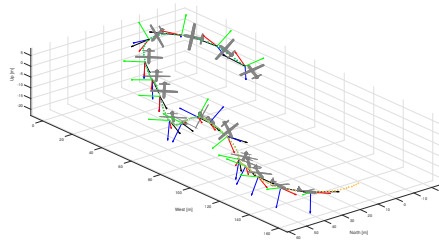


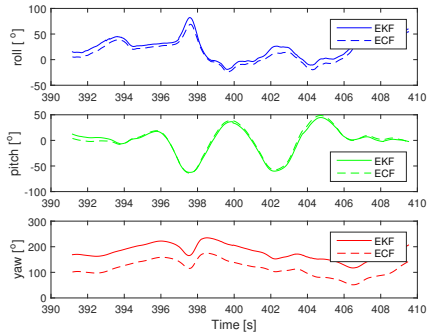
**Figure 7.14:** Entire flight, attitude and gyro biases.



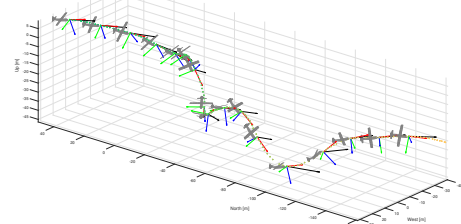
(a) Euler angles during roll manoeuvre.



(b) Visualised attitude and trajectory.

**Figure 7.15:** Attitude during roll manoeuvre.

(a) Euler angles during up and down accelerations/decelerations.



(b) Visualised attitude and trajectory.

**Figure 7.16:** Attitude during up and down accelerations/decelerations.

### 7.3.1 Acceleration Tests

Three methods are used in order to compensate for accelerations so that the accelerometer measurements can be relied on to a greater extent. These methods are discussed in Chapter 4.

The first method is the simplest method which is to simply throw away measurements where the norm deviates with  $\epsilon$  from 1 G. This gives reliable measurements during constant speeds but renders the accelerometer useless during longer accelerated motions which is why the EKF is tested during a coordinated turn. The second method uses differentiated velocity measurements from the GPS to estimate external accelerations. The third method makes use of these as well, but also uses angular rates from the gyroscope combined with GPS velocity measurements to estimate the centripetal acceleration. Both the GPS and the

accelerometer are LP filtered to  $\sim 5\text{Hz}$ .

The results of the different methods and the measurements rotated to the NED frame are presented in Figures 7.17, 7.18 and 7.19. Worth noting is that no vertical velocity measurements where available which has been solved by differentiating the altitude twice. Vertical velocity measurements would result in better estimates but the altitude differentiation proves to be quite accurate as well.

The results using method 1 can be seen in Figure 7.17. The figures show that the EKF is struggling during the manoeuvre.  $\epsilon$  is here set to 0.1 which is a rather large error value but still large parts of the measurements are thrown away. This indicates that the simplification that the accelerometer only measures gravity is largely inaccurate. The EKF still manages to estimate the attitude with some precision however. This is due to the gyro bias already being near the correct value which results in estimates matching the flight pattern quite well.

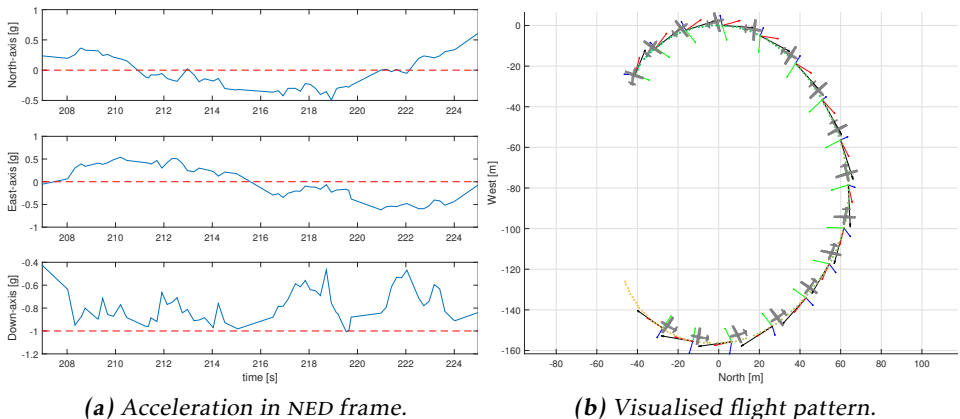
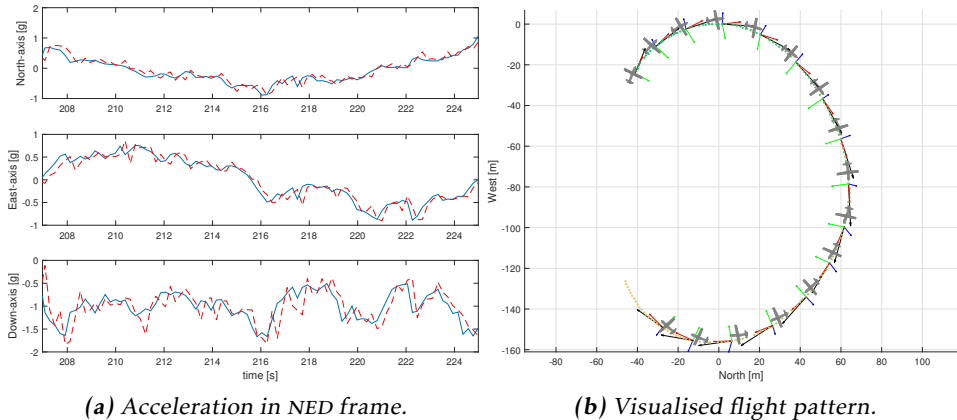


**Figure 7.17:** Results with no acceleration compensation.

The second method is presented in Figure 7.18. This result is a significant improvement compared to the previous method. The flight pattern looks reasonable and if the NED frame measurements are studied the GPS compensated acceleration and the accelerometer measurements are nearly aligned. The problem with this method is that the GPS has a delay that makes the estimated acceleration lag compared to the measurements from the accelerometer. The differentiation of velocity makes the estimation lag an additional sample. The result of this is clearly visible in Figure 7.18a. This problem should not produce large errors due to the fact that most accelerations are quite small and constant which makes the lag less of a problem than it can seem. It is still a large improvement over not estimating the acceleration at all.

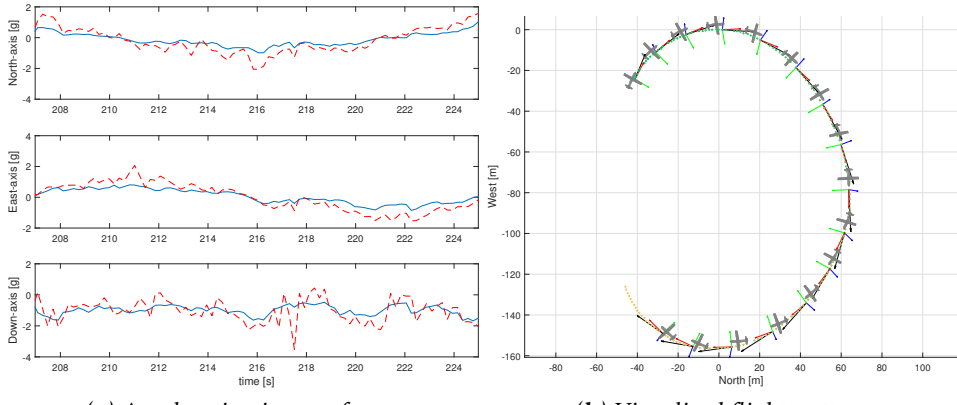
The third method which is shown in Figure 7.19 proves to be reliable when studying the flight pattern. However the NED frame measurements deviates to a larger degree compared to method 2 in Figure 7.18. This method should produce good results in theory as the GPS and the gyro together can estimate both linear and



**(a)** Acceleration in NED frame. **(b)** Visualised flight pattern.

**Figure 7.18:** Results with GPS calculated acceleration compensation.

centripetal accelerations. Studying the measurements in the NED frame however, it is clear that the method produce incorrect estimations of the acceleration. An alternative is to only use gyroscopes and velocity from GPS to estimate the centripetal motions but then no means of estimating linear acceleration is available. The problems with lag from differentiating the GPS is however remedied to some extent with this sort of compensation.



**(a)** Acceleration in NED frame. **(b)** Visualised flight pattern.

**Figure 7.19:** Results with GPS and gyro calculated acceleration compensation.

These three methods can all be used with quite good results. Method 2 is however the clear winner performance wise. This method demands high precision from the GPS and can not be used during dead reckoning where the first method has to be used.

### 7.3.2 Filter Convergence

Outlier detection and divergence monitoring is applied to the filter. Outlier detection is done with a high threshold, only removing the severely distorted measurements. The divergence monitoring is done with the exponential window approach with forgetting factor  $\lambda = 0.99$ . The resulting divergence test statistic during the flight in Figure 7.14 can be seen in Figure 7.20. As described in Section

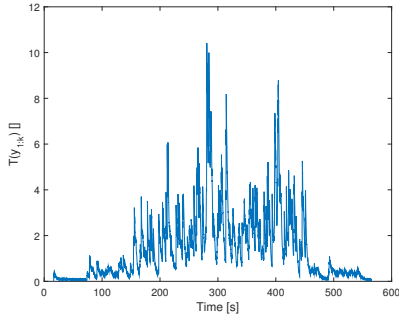


**Figure 7.20:** Divergence test statistic during flight.

5.4.1 the test indicates divergence if  $T \gg 1$ . This is not the case which indicates that the filter is convergent. The spikes are effects of accelerated motions where the used sensor models are insufficient. This is mostly fast accelerations which are hard to model properly. If unsuccessful the test statistic would not return to low values after spiking which also indicate that the filter converges. Most of the cases the applied models seem to manage well and the test is deemed as successful.

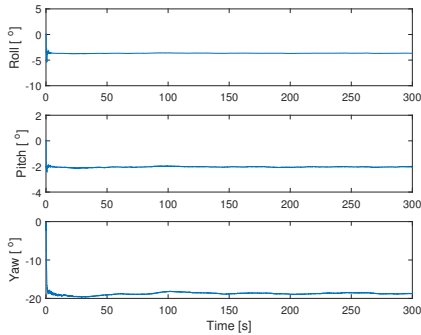
## 7.4 Implemented Filter

The c-implemented filter is tested through test bench and flight tests. No reference was available during the tests and the filter can only be evaluated visually. Another important factor, that determines whether the filter is successful or not, is if the Euler angles are correct at both start and end.

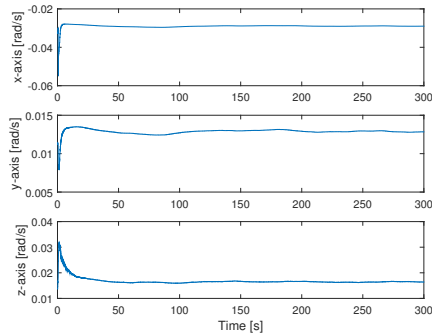
### 7.4.1 Test Bench

A static test is done in order to determine long term stability. This test can be seen in Figure 7.21 which shows that the filter is stable during the entire time.

The computation time of the filter during the same measurements can be seen in Figure 7.22 which shows that the computation time is not constant which is expected. Some fluctuations are dependant on which of the updates that are executed during this cycle. The mean of computation times of the time updates and



(a) Euler Angles during static measurements.



(b) Gyro biases during static measurements.

**Figure 7.21:** Results during static measurements.

the two measurement updates over 10000 cycles are seen in Table 7.1. Another reason for fluctuations is that there are some interrupts doing other calculations on the autopilot which take various amount of execution time.

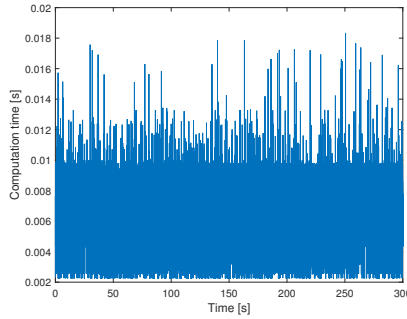


**Figure 7.22:** Computation time during static measurements.

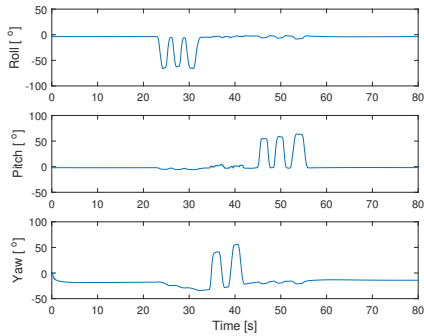
Test during simple movements are shown in Figure 7.23. As can be seen the movements affect the gyro biases. The angles are able to return to the nominal state after the movements indicating that the filter is performing as it should. The influence on the different angles from movement in other angles is because perfect rotation could not be achieved. The influence is however rather small and the overall performance can still be estimated.

## 7.4.2 Flight Tests

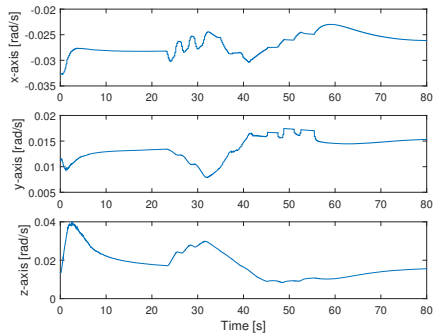
The c-implementation was tested during flights with the Spy Owl 100 fixed wing. No reference trajectory was available during the flights and hence the results are

**Table 7.1: Computation times**

Sample time	14.1941ms
Computation Time	6.3000 ms
Time Update	3.1791 ms
Magnetometer Measurement Update	2.6599 ms
Accelerometer Measurement Update	2.3513 ms



(a) Euler Angles during dynamics.

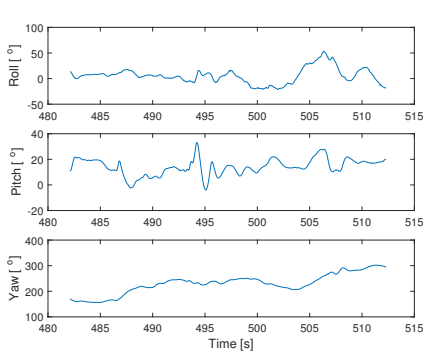


(b) Gyro biases during dynamics.

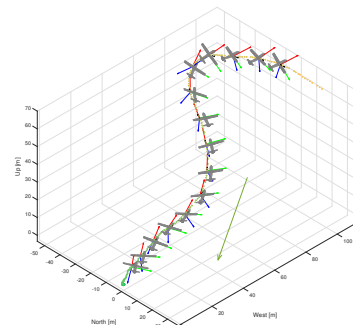
**Figure 7.23: Filter results during dynamics.**

evaluated visually. At the time of the tests there were winds over 10m/s. The Spy Owl 100 is sensitive to high winds which is why the plane is pointing in yaw angles which differ from the GPS trajectory when exposed to side winds. An important note to see whether the EKF is successful is to see if the attitude during launch and landing match. After the flight the aircraft was placed approximately in the same direction as it originated from which is another studied detail.

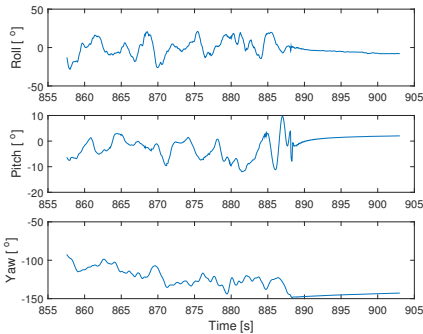
The attitude and trajectory during launch and landing are showed in Figures 7.24 and 7.25 respectively. Both launch and landing have reasonable trajectories. After launch the plane is exposed to strong side wind which makes the yaw angle almost perpendicular to the GPS-course. An approximate wind direction is visualised through a vector in the two plots.



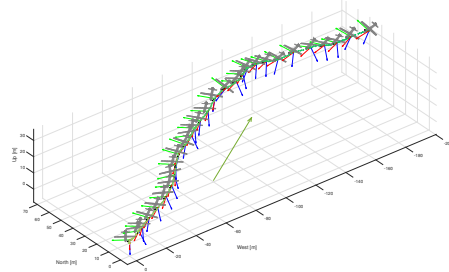
(a) Euler Angles during launch.



(b) Attitude and trajectory during launch.

**Figure 7.24:** Attitude during launch.

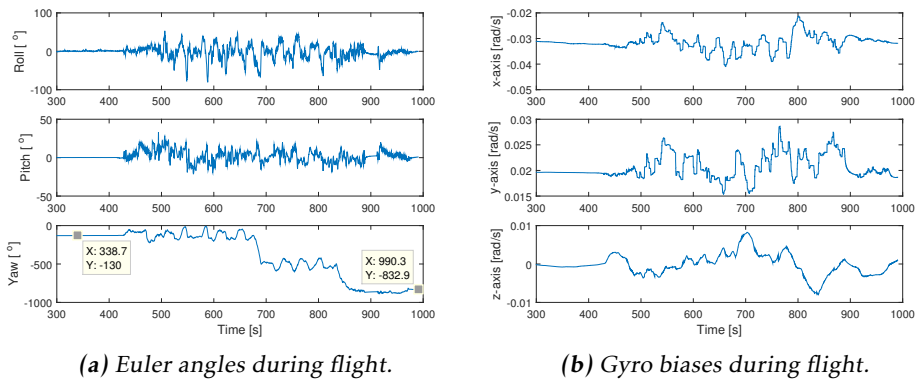
(a) Euler angles during landing.



(b) Attitude and trajectory during landing.

**Figure 7.25:** Attitude during landing.

The entire flight can be seen in Figure 7.26. As previously mentioned the plane was placed pointing in about the same direction as it started in. The figures show that the offset between starting and ending yaw angle is about  $17^\circ$ . Both roll and pitch are approximately  $0^\circ$  at both start and end of the logged flight. The placement of the plane was inexact, which is the most probable reason that the yaw angle is not exactly the same. Some drift in yaw angle might be another cause of error. However, since both launch and landing have reasonable attitude corresponding to the trajectories this drift is likely to be minimal. The gyro biases keep close to the values estimated while static on the ground during the flight indicating that the estimation is successful. The main reason for the changes in gyro bias estimation is due to model errors during fast accelerations. Small rotations and movements are likely to contribute to the accelerations measured by the accelerometer which the GPS-acceleration is not able to compensate for.



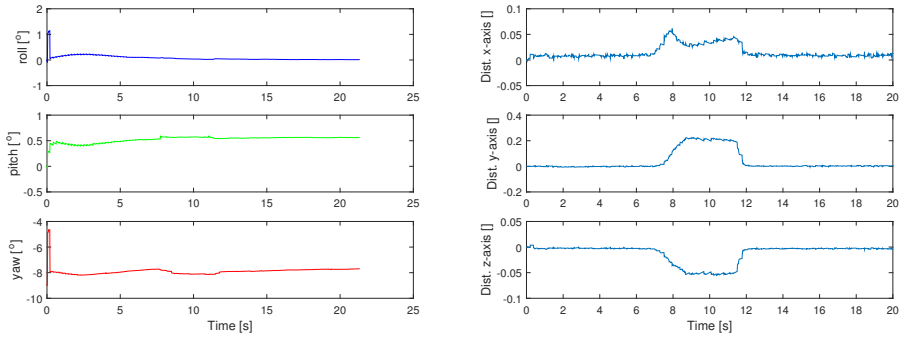
(a) Euler angles during flight.

(b) Gyro biases during flight.

**Figure 7.26:** Attitude and gyro biases during entire flight.

## 7.5 Magnetic Modelling

The magnetic modelling proposed in Section 4.6 performs quite well when data is logged during disturbance when the autopilot is static. The measurements are the same as in section Figure 7.3a but modelling is used instead of deciding when to use the magnetometer. The attitude using the method is presented in Figure 7.27a and the modelled disturbance is shown in Figure 7.27b.



(a) Euler angles using magnetic disturbance modelling.

(b) Modelled magnetic disturbance.

**Figure 7.27: Magnetic disturbance modelling.**

However when the autopilot is used in dynamic manoeuvres and the magnetometer is disturbed the method is struggling. The model is unable to determine what actually is a disturbance and what is movement of the sensor. This could be an issue with incorrect calibration of the magnetometer but is more likely to be a problem with the approach. The method is therefore not recommended for use in UAV applications and is not used in the final implementation of the filter. The performance of the model can also be a result of badly chosen parameters. There are three model parameters for the approach which makes it hard to tune.

## 7.6 Evaluation

The performance of the 7-state EKF is summarised here. The key features of the filter is discussed and the choice of final implementation is presented.

Due to the simplicity of the 7-state EKF it is able to meet the requirements in time efficiency while still being able to provide good results. The filter runs at about the same speed as the ECF solution in mean value but when both measurement updates and the time update are calculated during a single cycle the EKF is somewhat slower. This is of no consequence to the final results of the filter since the filter is running at a fast enough frequency.

On test bench the uncompensated filter is promising but it struggles somewhat during accelerations and disturbances. With compensation of accelerations from differentiated GPS measurements the filter is however significantly more robust and able to handle most situations . Fast accelerations is still an issue but does not impose large errors in the estimates. Even if the magnetometer is disturbed in flight the acceleration compensated EKF is able to estimate a correct yaw angle which the original filter is not able to. This however means that the UAV uses GPS measurements more and depends on good accuracy of those. During dead reckoning the EKF with no compensation of external accelerations has to be used. When the GPS compensation is used the covariance of the accelerometer measurement model is increased in order to compensate for the precision of the GPS measurements. This makes the filter converge at a slower rate during flight but compensates for noisy GPS measurements which would otherwise influence the measurements.

The magnetometer is easily disturbed which is why the magnetometer measurements are trusted less than the accelerometer measurements. Even so the magnetometer disturbances can lead to erroneous estimations. The magnetic disturbance in the implemented filter is detected by checking the norm of the measurements. The inclination is not checked due to the fact that the inclination angle depends on estimated orientation. However, if the calibration of the sensor is incorrect checking the norm and checking the inclination are both unsuccessful. Another important note is that the filter depends on a known magnetic declination.

Outlier rejection adds more robustness to the implemented filter as measurements that would otherwise produce errors in the estimates are dismissed. With carefully chosen parameters of measurement noise and outlier rejection filter convergence is achieved. Thresholds have been chosen through testing and have no statistical ground and could probably be tuned further.

The tested magnetic modelling proved to be less useful than theory suggests. The model is unable to differ between actual change in sensed field and disturbance. The model does however prove to have some of the sought functionality and if investigated further might be of use. An alternative to modelling the actual disturbance is to increase covariance with increasing errors in norm and inclination, which might be more applicable. In the final implemented filter none of these

methods are used as the GPS compensated accelerometer measurements are able to estimate the continuous change in yaw during flight. This means that the magnetometer covariance can be set to a high value allowing it to have affect during constant flight but not so during acrobatic flight where the accelerometer is used more.

With these things in mind the implemented EKF can after proper tuning provide reliable estimates of both attitude and gyro biases.

The EKF performs about the same as the ECF in estimating pitch and roll but outperforms the ECF in estimating yaw. The ECF also has stronger need of exact calibration as the gyro bias will make the estimates drift with time otherwise. Since the EKF models the gyro bias an improper calibration will only lead to small offsets as it is mostly accelerometer calibration which will contribute to the error. The EKF should after tuning also work on both helicopters and fixed wings due to the fact that GPS readings are used instead of pitot tubes when estimating external accelerations.

# 8

---

## Conclusion

This chapter concludes this thesis and presents further work and improvements which can be based on it.

### 8.1 Conclusions

A novel attitude algorithm has been presented in this thesis. Using an EKF with carefully chosen parameters the attitude quaternion and gyro biases can be estimated with high robustness. The robustness is achieved using differentiated GPS measurements to augment the accelerometer measurements model. This enables all of the Euler angles to be influenced by the accelerometer during accelerations rather than only the pitch and roll estimates.

A lot of time of the thesis work has been spent trying to determine the best use of the magnetometer. The conclusion is that the magnetometer is best used to update solely the yaw angle. This is due to the fact that the magnetometer is easily disturbed. The use of magnetometer also raises high demands on calibration as an erroneous calibration of the magnetometer can lead to the estimated yaw angle being far from the true value. However, due to the GPS compensated accelerations this can be remedied in flight which is why the filter utilises the accelerometer readings to greater extent than the magnetometer.

### 8.2 Future Work

This section covers additional work which could improve the outcome of this thesis.

### 8.2.1 UKF

Since filter divergence is a problem with the EKF the UKF might be a better choice in some situations. Since the computation time using the EKF leaves room to spare it would be interesting to see if the more computationally heavy UKF can be implemented on the same processor without violating speed requirements. The UKF does not need exact initialisation due to the fact that it can handle large initial uncertainty which the EKF can not.

### 8.2.2 Accelerometer Bias

The accelerometer bias changes with time. While this should only give a small offset to the estimated pitch and roll angles it would still be of interest to see if modelling of this bias can improve precision of the results.

### 8.2.3 Misalignment

The misalignment between magnetometer and accelerometer should be studied in even more detail. As the sensor equipment needed to determine the magnitude of this error was unavailable during the thesis it would be interesting to see what could be determined through proper measurement equipment.

### 8.2.4 Filter Monitor

The implemented monitor lacks physical interpretation. It would be of interest to study the divergence in greater detail and to know what leads to high divergence test statistics.

### 8.2.5 Magnetic Modelling

The modelling of magnetic disturbances was a sidetrack which proved to be more than challenging. It would be interesting to investigate further but due to the difficulty it could probably be the focus of an entire thesis.

# **Appendix**



# A

---

## Appendix A

### A.1 Transformations

When using the coordinate frames described in this chapter a way to transform coordinates in a given frame to another frame has to be used. The transformation between NED- and B-frame is covered in section 2.5 and the other necessary transformations are covered in this section.

#### A.1.1 Geodetic and ECEF

To be able to use GPS which is given in the *Geodetic frame* it has to be transformed to the ECEF as an intermediate step. The transformed coordinate in ECEF is described in Cai et al. [2011] and is given by

$$P_e = \begin{bmatrix} x_e \\ y_e \\ z_e \end{bmatrix} = \begin{bmatrix} (N_E + h) \cos \varphi \cos \lambda \\ (N_E + h) \cos \varphi \sin \lambda \\ (N_E(1 - e^2) + h) \sin \varphi \end{bmatrix} \quad (\text{A.1})$$

where  $N_E$  and  $e$  are given in table 2.1.

#### A.1.2 ECEF to NED

The transformation from ECEF to local NED is given by

$$P_n = R_{n/e}(P_e - P_{e,ref}) \quad (\text{A.2})$$

where  $P_{e,ref}$  is the local reference origin and  $R_{n/e}$  is given by

$$R_{n/e} = \begin{bmatrix} -\sin \varphi_{ref} \cos \lambda_{ref} & -\sin \varphi_{ref} \sin \lambda_{ref} & \cos \varphi_{ref} \\ -\sin \lambda_{ref} & \cos \lambda_{ref} & 0 \\ -\cos \varphi_{ref} \cos \lambda_{ref} & -\cos \varphi_{ref} \sin \lambda_{ref} & -\sin \varphi_{ref} \end{bmatrix}. \quad (\text{A.3})$$

Here  $\lambda_{ref}$   $\varphi_{ref}$  are latitude and longitude of  $P_{e,ref}$  in the geodetic frame.

---

## Bibliography

Vibhor L. Bageshwar, Demoz Gebre-Egziabher, William L. Garrard, and Tryphon T. Georgiou. A stochastic observability test for discrete-time kalman filters. Technical report, University of Minnesota Minneapolis, 2009. Cited on page 52.

Martin Barczyk. *Nonlinear State Estimation and Modeling of a Helicopter UAV*. PhD thesis, Department of Electrical and Computer Engineering , University of Alberta, 2012. URL <http://hdl.handle.net/10402/era.25264>. Cited on page 14.

Leandro Baroni and Hélio Koiti Kuga. Analysis of attitude determination methods using gps carrier phase measurements. *Mathematical Problems in Engineering*, vol. 2012, Article ID 596396, 10 pages, 2012. doi: doi:10.1155/2012/596396. Cited on page 4.

G. Cai, B.M. Chen, and T.H. Lee. *Unmanned Rotorcraft Systems*. Advances in Industrial Control. Springer, 2011. ISBN 9780857296351. Cited on pages 8, 10, and 81.

J. L. Crassidis, F. L. Markley, and Y. Cheng. Survey of Nonlinear Attitude Estimation Methods. *Journal of Guidance Control Dynamics*, 30:12–28, January 2007. doi: 10.2514/1.22452. Cited on page 1.

H.G. de Marina, F.J. Pereda, J.M. Giron-Sierra, and F. Espinosa. Uav attitude estimation using unscented kalman filter and triad. *Industrial Electronics, IEEE Transactions on*, 59(11):4465–4474, Nov 2012. ISSN 0278-0046. doi: 10.1109/TIE.2011.2163913. Cited on page 1.

Gabriel Elkaim. Misalignment calibration using body frame measurements. American Control Conference, ACC13, Washington D.C., 2013. Cited on page 18.

Fredrik Gustafsson. *Statistical Sensor Fusion*, volume 2:1. Studentlitteratur AB, 2012. ISBN 978-91-44-07732-1. Cited on pages 49, 50, 52, and 53.

- Fredrik Gustafsson, Lennart Ljung, and Mille Millnert. *Signal Processing*, volume 1:3. Studentlitteratur AB, 2011. ISBN 978-91-44-07732-1. Cited on page 43.
- Fredrik Johansson and Hugo Kinner. Sensorfusion för reglering av obemannad helikopter. Master's thesis, Linköping University, Automatic Control, The Institute of Technology, 2011. Cited on pages 2, 18, 20, and 32.
- Jung Keun Lee, E.J. Park, and S.N. Robinovitch. Estimation of attitude and external acceleration using inertial sensor measurement during various dynamic conditions. *Instrumentation and Measurement, IEEE Transactions on*, 61(8): 2262–2273, Aug 2012. ISSN 0018-9456. doi: 10.1109/TIM.2012.2187245. Cited on page 42.
- R.R. Lima and L.A.B. Torres. Performance evaluation of attitude estimation algorithms in the design of an ahrs for fixed wing uavs. In *Robotics Symposium and Latin American Robotics Symposium (SBR-LARS), 2012 Brazilian*, pages 255–260, Oct 2012. doi: 10.1109/SBR-LARS.2012.61. Cited on pages 2, 42, and 46.
- Sebastian O.H. Madwick. An efficient orientation filter for inertial and inertial/magnetic sensor arrays. Technical report, April 2010. Cited on page 45.
- Thom Magnusson. State estimation of uav using extended kalman filter. Master's thesis, Linköping University, Automatic Control, The Institute of Technology, 2013. Cited on pages 2, 32, 33, and 42.
- Henrik Rehbinder and Xiaoming Hu. Drift-free attitude estimation for accelerated rigid bodies. *Automatica*, 40(4):653 – 659, 2004. ISSN 0005-1098. doi: <http://dx.doi.org/10.1016/j.automatica.2003.11.002>. URL <http://www.sciencedirect.com/science/article/pii/S0005109803003595>. Cited on page 46.
- Valérie Renaudin, Muhammad Haris Afzal, and Gérard Lachapelle. Complete triaxis magnetometer calibration in the magnetic domain. *Journal of Sensors*, 2010, Article ID 967245, 2010. Cited on pages 30, 31, and 32.
- Daniel Roetenberg, Henk J. Luinge, Chris T. M. Baten, and Peter H. Veltink. Compensation of magnetic disturbances improves inertial and magnetic sensing of human body segment orientation. *IEEE Transactions on Neural Systems and Rehabilitation Engineering, [see also IEEE Transactions on Rehabilitation Engineering]*, 13:395–405, 2005. Cited on page 47.
- V. Sazdovski, P.M.G. Silson, and A. Tsourdos. Attitude determination from single camera vector observations. In *Intelligent Systems (IS), 2010 5th IEEE International Conference*, pages 49–54, July 2010. doi: 10.1109/IS.2010.5548331. Cited on page 4.
- Isaac Skog and Peter Hänel. Calibration of a mems inertial measurement unit. In *in Proc. XVII IMEKO WORLD CONGRESS, (Rio de Janeiro)*, 2006. Cited on page 25.

- Steven W. Smith. *The Scientist and Engineer's Guide to Digital Signal Processing*. California Technical Publishing, San Diego, CA, USA, 1997. ISBN 0-9660176-3-3. Cited on page 39.
- Kian Sek Tee, Mohammed Awad, Abbas Dehghani, David Moser, and Saeed Zadehi. Triaxial accelerometer static calibration. In *Proceedings of the World Congress on Engineering*, volume 3, 2011. Cited on pages 25, 27, and 28.
- D. Titterton, J.L. Weston, and Institution of Electrical Engineers. *Strapdown Inertial Navigation Technology, 2nd Edition*. IEE radar, sonar, navigation, and avionics series. Institution of Engineering and Technology, 2004. ISBN 9780863413582. Cited on pages 12, 13, 14, 15, and 23.
- David Törnqvist. Statistical fault detection with applications to imu disturbances, 2006. Cited on pages 41 and 44.
- Clas Veibäck. Automatic control of unmanned aerial vehicles. Master's thesis, Uppsala University, 2010. Cited on pages 5 and 6.
- Oliver J. Woodman. An introduction to inertial navigation. Technical Report UCAM-CL-TR-696, University of Cambridge, Computer Laboratory, August 2007. URL <http://www.cl.cam.ac.uk/techreports/UCAM-CL-TR-696.pdf>. Cited on page 20.
- J.M. Zogg and U-Blox. *GPS: Essentials of Satellite Navigation : Compendium : Theorie and Principles of Satellite Navigation, Overview of GPS/GNSS Systems and Applications*. U-Blox, 2009. ISBN 9783033021396. URL [https://www.u-blox.com/images/downloads/Product\\_Docs/GPS\\_CompPENDIUM%28GPS-X-02007%29.pdf](https://www.u-blox.com/images/downloads/Product_Docs/GPS_CompPENDIUM%28GPS-X-02007%29.pdf). Cited on pages 35 and 36.

---



## Upphovsrätt

Detta dokument hålls tillgängligt på Internet — eller dess framtida ersättare — under 25 år från publiceringsdatum under förutsättning att inga extraordinära omständigheter uppstår.

Tillgång till dokumentet innebär tillstånd för var och en att läsa, ladda ner, skriva ut enstaka kopior för enskilt bruk och att använda det oförändrat för icke-kommersiell forskning och för undervisning. Överföring av upphovsrätten vid en senare tidpunkt kan inte upphäva detta tillstånd. All annan användning av dokumentet kräver upphovsmannens medgivande. För att garantera äktheten, säkerheten och tillgängligheten finns det lösningar av teknisk och administrativ art.

Upphovsmannens ideella rätt innehåller rätt att bli nämnd som upphovsman i den omfattning som god sed kräver vid användning av dokumentet på ovan beskrivna sätt samt skydd mot att dokumentet ändras eller presenteras i sådan form eller i sådant sammanhang som är kränkande för upphovsmannens litterära eller konstnärliga anseende eller egenart.

För ytterligare information om Linköping University Electronic Press se förlagets hemsida <http://www.ep.liu.se/>

## Copyright

The publishers will keep this document online on the Internet — or its possible replacement — for a period of 25 years from the date of publication barring exceptional circumstances.

The online availability of the document implies a permanent permission for anyone to read, to download, to print out single copies for his/her own use and to use it unchanged for any non-commercial research and educational purpose. Subsequent transfers of copyright cannot revoke this permission. All other uses of the document are conditional on the consent of the copyright owner. The publisher has taken technical and administrative measures to assure authenticity, security and accessibility.

According to intellectual property law the author has the right to be mentioned when his/her work is accessed as described above and to be protected against infringement.

For additional information about the Linköping University Electronic Press and its procedures for publication and for assurance of document integrity, please refer to its www home page: <http://www.ep.liu.se/>